Linking bioenergetic function of mitochondria to tissue-specific molecular fingerprints

Running Head: Physiological diversity of mitochondria

Lisa Kappler[1], Miriam Hoene[1], Chunxiu Hu[2], Christine von Toerne[3], Jia Li[1,4], Daniel Bleher[1], Christoph Hoffmann[1], Anja Böhm[5,6], Laxmikanth Kollipara[7], Hans Zischka[8,9], Alfred Königsrainer[10,11], Hans-Ulrich Häring[1,5,6], Andreas Peter[1,5,6], Guowang Xu[2], Albert Sickmann[7,12,13], Stefanie M Hauck[3,6], Cora Weigert[1,5,6], Rainer Lehmann[1,5,6*]

[1]*Institute for Clinical Chemistry and Pathobiochemistry, Department for Diagnostic Laboratory Medicine, University Hospital Tuebingen, Tuebingen, Germany*

[2]*CAS Key Laboratory of Separation Science for Analytical Chemistry, Dalian Institute of Chemical Physics, Chinese Academy of Sciences, Dalian, China*

[3]*Research Unit Protein Science, Helmholtz Center Munich, Munich, Germany*

[4]*Key Laboratory of Tea Biology and Resources Utilization, Ministry of Agriculture, Tea Research Institute, Chinese Academy of Agricultural Sciences, Hangzhou 310008, China*

[5]*Institute for Diabetes Research and Metabolic Diseases of the Helmholtz Center Munich at the University of Tuebingen, Tuebingen, Germany*

[6]*German Center for Diabetes Research (DZD)*

[7]*Leibniz-Institut für Analytische Wissenschaften - ISAS - e.V., Dortmund, Germany*

[8]*Institute of Molecular Toxicology and Pharmacology, Helmholtz Center Munich, German Research Center for Environmental Health GmbH, Neuherberg, Germany*

[9]*Institute of Toxicology and Environmental Hygiene, Technical University Munich, Munich, Germany*

[10]*Department of General, Visceral and Transplant Surgery, University Hospital Tuebingen, Tuebingen, Germany*

[11]*German Cancer Consortium (DKTK) and German Cancer Research Center (DKFZ) partner site, Tuebingen, Germany*

[12]*Medizinisches Proteom-Center (MPC), Ruhr-Universität Bochum, Bochum, Germany*

[13]*Department of Chemistry, College of Physical Sciences, University of Aberdeen, Aberdeen, United Kingdom*

***Corresponding Author:**

Prof. Dr. Rainer Lehmann,

Clinical Chemistry Central Laboratory,

Department of Diagnostic Laboratory Medicine,

University Hospital Tuebingen,

Hoppe-Seyler-Str.3,

72076 Tuebingen

Germany

E-Mail: rainer.lehmann@med.uni-tuebingen.de

Phone: 0049 (0)7071 29 83193

ABSTRACT

Mitochondria are dynamic organelles with diverse functions in tissues such as liver and skeletal muscle. To unravel the mitochondrial contribution to tissue-specific physiology, we performed a systematic comparison of the mitochondrial proteome and lipidome and assessed the consequences hereof for respiration. Liver and skeletal muscle mitochondrial protein composition was studied by data-independent UHPLC-MS/MS-proteomics, lipid profiles were compared by UHPLC-MS/MS lipidomics. Mitochondrial function was investigated by high-resolution respirometry in samples from mice and humans. Enzymes of pyruvate oxidation as well as several subunits of complex I, III, and ATP synthase were more abundant in muscle mitochondria. Muscle mitochondria were enriched in cardiolipins associated with higher oxidative phosphorylation capacity and flexibility, in particular CL(18:2)$_4$ and 22:6-containing cardiolipins. In contrast, protein equipment of liver mitochondria indicated a shuttling of complex I substrates towards gluconeogenesis and ketogenesis and a higher preference for electron transfer via the flavoprotein quinone oxidoreductase pathway. Concordantly, muscle and liver mitochondria showed distinct respiratory substrate preferences. Muscle respired significantly more on the complex I substrates pyruvate and glutamate, while in liver maximal respiration was supported by complex II substrate succinate. This was a consistent finding in mouse liver and skeletal muscle mitochondria and human samples. Muscle mitochondria are tailored to produce ATP with a high capacity for complex I-linked substrates. Liver mitochondria are more connected to biosynthetic pathways, preferring fatty acids and succinate for oxidation. The physiologic diversity of mitochondria may be the key to tissue-specific disease pathologies and to therapies targeting mitochondrial function.

Keywords:

Cardiolipins, liver, mitochondria, muscle, substrate preference

1. INTRODUCTION

Mitochondria are in the focus of basic and translational research due to their central metabolic function and their involvement in the pathophysiology of human diseases such as neurodegenerative disorders, cancer and diabetes (53). Even though it is evident that mitochondria must be well adapted for the different functions of organs in metabolism, only few studies report tissue-specific characteristics and most of these studies just focus on one aspect such as mitochondrial morphology, protein abundance and oxidative capacity (3, 19, 24, 34). Mitochondria and their function are often rather generalized among tissues and mitochondrial (dys)function is examined in disease pathologies without paying attention to probable tissue specificities. We believe that the investigation of the specific mitochondrial characteristics in disease-related tissues might lead to more specific and thus effective understanding and thinking forward treatments of mitochondria-related diseases.

Two types of molecules are the central executors and regulators of mitochondrial function: proteins and lipids. Since proteins perform almost all relevant metabolic conversions in mitochondria, determination of protein abundances in different tissues is the first step to understanding the molecular determinants of the divergent metabolic activities adapted specifically to diverse cellular and tissue requirements. Lipids on the other hand, in addition to being a membrane constituent and energy source, are involved in physiological processes such as mitochondrial fusion and fission, fine-tune membrane structure and fluidity, and participate in electron transport chain assemblage, protein biogenesis, apoptosis and many other processes (6, 17, 35). Taken together, lipids regulate mitochondrial function on many levels and changes in lipid homeostasis and membrane composition are very likely to regulate both mitochondrial structure and function (14, 17). We started our tissue-specific investigation of mitochondria with skeletal muscle and liver, two insulin target tissues playing a central role in the origin and progression of diabetes. A (dys)function of mitochondria in these tissues is often discussed as central to diabetes development (22, 23, 33, 41).

Skeletal muscle and liver mitochondria have quite distinctly different physiological tasks. Mitochondria in skeletal muscle face large variances in ATP demands upon physical activity, requiring

91 greater variations in the rate of metabolism than any other tissue. Skeletal muscle is responsible for
92 over 80% of postprandial glucose disposal (7), and is furthermore considered to be the major organ
93 for fatty acid disposal because of its relative size in men and most animals (11). Liver on the other
94 side balances supply and blood concentration of glucose by the release of glucose from
95 glycogenolysis and gluconeogenesis. Liver contributes to a major extent to total glucose
96 production (43), and it is the major site of fatty acid production in humans (38). Intrahepatic fatty
97 acids are used for oxidation, storage or for packaging them into lipoproteins for export and storage
98 or use in other tissues (42). In states of prolonged exercise or fasting, hepatic mitochondrial
99 ketogenesis provides acetoacetate and 3-hydroxybutyrate as substrates for peripheral tissues like the
100 skeletal muscle, but also brain and heart (29).

101 We hypothesize that these major differences in metabolic pathways are reflected by differences in
102 both mitochondrial protein equipment and lipid composition of liver and skeletal muscle with
103 consequences on respiratory function. Therefore, we applied a systemic approach combining
104 proteomics and lipidomics analyses with high-resolution respirometry to understand tissue-specific
105 mitochondrial function and organization. Tissue-specific physiological diversity was revealed in
106 hepatic and skeletal muscle mitochondria from mice and validated in human samples.

107

108 **2. MATERIALS AND METHODS**

109 **2.1 Chemicals**

110 Bradford Reagent was from Carl Roth (Karlsruhe, Germany). Infrared fluorescent dye secondary
111 antibodies (anti-mouse/-rabbit/-guinea pig) were purchased from LI-COR (Lincoln, NE, USA). Anti-
112 ACADM (sc-365448) and anti-ODP (sc377092) were from Santa Cruz Biotechnology Inc. (Dallas, TX,
113 USA). Anti-pyruvate carboxylase (SAB2500845) was purchased from Sigma-Aldrich (Munich,
114 Germany). Anti-OXPHOS-Cocktail (ab110413), anti-citrate synthase (ab96600) and anti-ECHA
115 (ab54477) antibodies were purchased from Abcam (Cambridge, UK). The anti-COX4 antibody (4844S)

was purchased from Cell Signaling Technology (Danvers, MA, USA). MS or LC grade solvents acetonitrile (ACN), methanol (MeOH) and isopropanol (IPA) were purchased from Merck (Darmstadt, Germany). Ammonium acetate was purchased from Sigma-Aldrich (Munich, Germany). Ultra-pure water was prepared by a Milli-Q system (Millipore, MA, USA). The synthetic lipid standards d4-palmitic acid, CER(d18:1/17:0), LPC(19:0), $PC(19:0)_2$, $PE(15:0)_2$, SM(d18:1/12:0), $TG(15:0)_3$, $CL(14:0)_4$, $CL(14:1)(24:1)_3$, $CL(14:1)_3(15:1)$, $CL(15:0)_3(16:1)$ and $CL(14:1)(22:1)_3$ were purchased from Avanti Polar Lipids (Alabaster, AL, USA) or Sigma-Aldrich (Munich, Germany). High-resolution-respirometry substrates and inhibitors antimycin A, carbonylcyanide p-trifluoromethoxyphenylhydrazone (FCCP), cytochrome c, malate, pyruvate, rotenone, and succinate were purchased from Sigma-Aldrich (Munich, Germany). Adenosine diphosphate was purchased from Calbiochem, Merck (Darmstadt, Germany) and octanoylcarnitine from Tocris Bioscience (Bristol, UK).

2.2 Methods

2.2.1 Animal care

The animal experiment was performed in accordance with the Directive 2010/63/EU of the European Union and the German Animal Welfare Act and approved by the local authorities (Regierungspraesidium Tuebingen). Investigations were performed in tissues of 18-week-old male C57Bl/6N mice. Mice were purchased from Charles River (Sulzfeld, Germany) at an age of 9 weeks and fed a purified standard diet (E157453-04, Ssniff, Soest, Germany) ad libitum. For organ harvesting, mice were analgosedated with an intraperitoneal injection of ketamine and xylazine (150 and 10 mg/kg body weight, respectively), and exsanguinated by decapitation.

2.2.2 Human samples

Skeletal muscle biopsies were obtained by percutaneous needle biopsies performed on the vastus lateralis of the quadriceps femoris after local anesthesia (2% Scandicaine; Aspen Pharma GmbH, Munich, Germany) from participants who completed an exercise intervention study. Informed written consent was given by all individuals; the study protocol was approved by the ethics

committee of the University of Tuebingen (446/2016BO2) and was in accordance with the Declaration of Helsinki. The fresh human liver tissue was collected during hepatic surgery that was performed for different reasons, e.g., hepatic haemangioma, curative resection of hepatic metastases of colorectal malignancies or hepatocellular carcinoma, at the Department of General, Visceral, and Transplant Surgery at the University Hospital of Tuebingen. Only samples from normal, non-diseased tissue were used. Patients fasted overnight before collection of liver samples. Exclusion criteria were viral hepatitis infection and liver cirrhosis. Informed, written consent was obtained from all participants, and the ethics committee of the University of Tuebingen approved the protocol (239/2013BO1) that was in accordance with the Declaration of Helsinki.

2.2.3 Mitochondria isolation

Mitochondria isolation was performed as previously described (21) with some modifications. A scheme of the experimental workflow is given in Supplementary Figure A.1. All isolation steps were performed at 4 °C or on ice. The homogenisation procedure was different for each tissue: 150 mg liver were directly placed into ice-cold STE buffer (250 mM sucrose, 5 mM Tris, 2 mM EGTA, 0.5% BSA, pH 7.4 at 4 °C). Tissue was cut into small pieces, homogenized using a loosely fitted 2 ml glass-glass douncer (Sartorius, Goettingen, Germany) by applying 6 strokes, transferred to a 50 ml tube, and filled up with STE + 0.5% BSA. For the homogenisation of muscle, 550 mg pooled upper hind limb skeletal muscle tissue (mostly type 2 fibers) were directly transferred into ice-cold phosphate-buffered saline (PBS; Sigma-Aldrich, Munich, Germany). Tissue was cut into small pieces, transferred to a 50 ml tube and digested for 3 min at 4 °C with type VIII protease from *Bacillus licheniformis* (Sigma-Aldrich, Munich, Germany). 1 ml enzyme solution (6 mg protease (10 U/mg) per ml STE) was added to 100 mg tissue. After 3 min, 10 ml STE + 0.1% BSA were added and the sample was centrifuged for 30 s at 900 g at 4 °C. Supernatant was removed, the tube filled up with STE + 0.1% BSA and centrifuged again. This washing step was repeated 3 times in total. The muscle suspension was then homogenized using a 15 ml teflon-glass douncer (Sartorius, Goettingen, Germany). After the tissue-specific homogenisation procedure, all following centrifugation steps and procedures were

similar for both homogenates. The homogenates were centrifuged at 900 g for 10 min. The supernatant was transferred into a new centrifuge tube and centrifugation was repeated. The supernatant was then centrifuged at 9 000 g for 10 min to pellet the crude mitochondrial fraction. The pellet was resuspended in STE + 0.1% BSA and centrifuged again at 9 000 g for 10 min. The crude mitochondrial pellet was carefully resuspended in 200 µl STE. An aliquot was used to determine the total protein concentration using Bradford reagent. 100 µg of this mitochondrial suspension were used for respiration analyses as described below. The remaining mitochondrial suspension was layered on 5 ml percoll gradient (25%) and centrifuged for 20 min at 80 000 g. The lower of the two appearing layers was collected with a Pasteur pipette and transferred to a new centrifuge tube, filled up with STE without BSA and centrifuged 10 min at 9 000 g. The pellet was resuspended in a small volume of STE buffer without BSA. After centrifugation at 16 000 g for 2 min the supernatant was removed, the pellet was resuspended in PBS and protein concentration was determined using BCA assay (Pierce™ BCA Protein Assay Kit, Rockford, USA). Aliquots with specific protein amounts for lipidomics, western blotting and proteomics were frozen at -80 °C.

2.2.4 Tissue lysis, electrophoresis and western blot analysis

For whole-tissue western blot analysis mouse liver and skeletal muscle tissue was homogenized in cold 1 ml RIPA lysis buffer (25 mM Tris, 150 mM NaCl, 0.1% SDS, 0.5% NaDOC, 1% Triton-X-100; pH 7.6) using a TissueLyser (Qiagen, Hilden, Germany). The settings were 2 min at 20 Hz for liver and 4 min at 20 Hz for muscle tissue. The lysate was centrifuged for 10 min at 13 000 g at 4 °C. Supernatant was transferred to a new cup and centrifugation was repeated. The supernatant from the second centrifugation was aliquoted and stored at -80 °C. Immunoblots from 30 µg of protein from tissue lysate or isolated mitochondrial fraction were performed as described (21) using IRDye® secondary antibodies (LI-COR Biosciences GmbH, Bad Homburg, Germany).

2.2.5 Proteomic sample preparation

Ten µg of sample were subjected to tryptic digest using a modified filter-aided sample preparation protocol (13, 54) with the following changes: a buffer was added to each sample containing urea and SDS in a final concentration of 4 M and 2%, respectively. Samples were reduced at RT. Peptides were stored at -80°C until MS measurement.

2.2.6 UHPLC-MS/MS-Proteomics

MS measurements were performed in data independent (DIA) mode. MS data were acquired on a Q Exactive (QE) high field (HF) mass spectrometer (Thermo Fisher Scientific, Rockford, IL, USA). Approximately 0.5 µg per sample were automatically loaded to the online coupled RSLC (Ultimate 3000, Thermo Fisher Scientific Inc.) HPLC system. A nano trap column was used (300 µm inner diameter × 5 mm, packed with Acclaim PepMap100 C18, 5 µm, 100 Å; LC Packings, Sunnyvale, CA) before separation by reversed phase chromatography (Acquity UHPLC M-Class HSS T3 Column 75µm ID x 250mm, 1.8µm; Waters, Eschborn, Germany) at 40°C. Peptides were eluted from column at 250 nl/min using increasing ACN concentration (in 0.1% formic acid) from 3% to 41% over a 105 minutes gradient. The DIA method consisted of a survey scan from 300 to 1650 m/z at 120 000 resolution and an automatic gain control (AGC) target of 3e6 or 120 ms maximum injection time. Fragmentation was performed via higher energy collisional dissociation (HCD) with a target value of 3e6 ions determined with predictive AGC. Precursor peptides were isolated with 37 variable windows spanning from 300 to 1650 m/z at 30 000 resolution with an AGC target of 3e6 and automatic injection time. The normalized collision energy was 28 and the spectra were recorded in profile mode. To generate the peptide spectral library, selected LC-MS/MS data dependent acquisition data encompassing 164 raw files were analysed using Proteome Discoverer (Version 2.1, ThermoFisher Scientific) using Byonic (Version 2.0, Proteinmetrics, San Carlos, CA) search engine node maintaining 1% peptide and protein FDR threshold. The library was generated in Spectronaut (Version 10, Biognosys, Schlieren, Switzerland) with default settings using the Proteome Discoverer result file. Spectronaut was equipped with the Swissprot mouse database (Release 2017.02, 16869 sequences, www.uniprot.org)

with a few spiked proteins (e.g., Biognosys iRT peptide sequences). The final spectral library generated in Spectronaut contained 10525 protein groups and 322041 peptide precursors. The DIA MS data was analysed for muscle and liver together using the Spectronaut 10 software applying default settings with the following exceptions: Quantification was limited to proteotypic peptides, data filtering was set to Qvalue 50% percentile, summing up peptide abundances. To compensate for overall differences in protein abundance, intensities of individual proteins were normalized to total protein content of the respective sample. To estimate the purity of the mitochondrial fractions, proteomics data were queried against the Mitominer database (Mitominer 4.0 (48)), query was performed based on gene symbols.

2.2.7 Sample preparation for lipidomics

Lipids were extracted with methyl tert-butyl ether (MTBE) as described previously (5). Briefly, water was added to 50 µg (by protein) of mitochondrial suspension to reach a total volume of 100 µl. Next, 350 µl of ice-cold methanol including internal standards were added. Samples were briefly vortexed, 1 ml of MTBE was added, and the samples were shaken for 30 min at room temperature. After adding 250 µl of water and incubating the sample at room temperature for 10 min, samples were centrifuged for 20 min at 1 000 g and 4 °C to induce phase separation.

2.2.8 UHPLC-MS/MS-lipidomics

Lipidomics profiling was performed in a Waters UHPLC system (Milford, MA, USA) coupled with a Q Exactive (QE) high field (HF) mass spectrometer (Thermo Fisher Scientific, Rockford, IL, USA). Separation of lipid metabolites was achieved in a Waters UHPLC C8 ACQUITY column (100 mm x 2.1 mm × 1.7 µm) (Milford, MA, USA). The elution solvents consisted of A (acetonitrile (ACN):H_2O = 60:40, v/v) and B (isopropanol:ACN = 90:10, v/v), both containing 10 mM ammonium acetate. The elution gradient started at 32% B for the initial 1.5 min, followed by a linear increase to 85% B during the next 14 min. Within the subsequent 0.1 min, solvent B was rapidly increased to 97%, and then maintained for 2.4 min for column flush. Subsequently, the elution solvent was returned to 32% B within 0.1 min and kept for 1.9 min for column equilibration. The column

temperature was set to 55 °C and the flow rate was 0.26 ml/min. Lipidomics data were acquired in both ESI positive and negative modes at scan ranges of 400 –1300 Da and 200 – 1 800 Da, respectively. The spray voltage was 3.5 kV for positive mode and -3.0 kV for negative mode. The capillary temperature was maintained at 300 °C. The auxiliary gas heater temperature was set to 350 °C. The flow rate of sheath gas and auxiliary gas was 45 arbitrary units (arb) and 10 arb, respectively. The S-lens RF level was 50. The AGC target was set to be 3×10^6 ion capacity and maximum IT was 200 ms. Mass resolution was 120 000 and 30 000 for full scan MS and data-dependent MS/MS. Lipid identities were assigned based on accurate mass measurement, MS/MS fragmentation and LC elution behavior. 95% of all detected lipids showed a RSD below 20% throughout nine injections of a pooled sample during the whole UHPLC-MS run. All detected lipids were quantified by normalization to the corresponding internal standard.

2.2.9 Functional assay

Mitochondrial function was investigated by respiration measurements in an Oxygraph-2k (Oroboros Instruments, Innsbruck, Austria). 100 µg of the crude mitochondrial suspension were placed in Mir05 buffer (0.5 mM EGTA, 3 mM $MgCl_2(H_2O)_6$, 60 mM K-lactobionate, 20 mM taurine, 10 mM KH_2PO_4, 20 mM HEPES, 110 mM sucrose, 1 g/l BSA, pH=7.1 at 30 °C) in the Oxygraph-2k chambers. 1.28 mM malate, 0.5 mM octanoylcarnitine (fatty acid oxidation, FAO), 2.5 mM ADP (phosphorylating condition), 5 mM pyruvate or 10 mM glutamate (complex I respiration), 2.5 mM succinate (complex II respiration), 10 µM cytochrome c (integrity control), FCCP in 0.5 µM steps (uncoupled state), 1.25 µM rotenone (complex I inhibitor) and 5 µM antimycin A (complex III inhibitor) were added to evaluate electron transport chain capacity and non-mitochondrial oxygen consumption. Cytochrome c effect as control for integrity was 18.1±3.6% for liver mitochondria and 4.5±2.1% for muscle mitochondria. Liver and muscle mitochondria were isolated from tissues of the same animal. Further experiments were 1.28 mM malate, 5 mM pyruvate or 10 mM glutamate, 2.5 mM ADP, 0.5 mM octanoylcarnitine, 10 µM cytochrome c (integrity control), FCCP in 0.5 µM steps (uncoupled state),

1.25 µM rotenone (complex I inhibitor) and 5 µM antimycin A (complex III inhibitor). Data was corrected for non-mitochondrial background by subtraction of antimycin A oxygen consumption.

2.2.10 Respiratory measurements of human samples

Muscle fibers were skinned as previously published by Pesta and Gnaiger (39) with modifications. Muscle biopsies were directly placed in the Mir05 buffer. During skinning of the fibers in a six-well plate, the dissected fibers were placed in a 70 µm cell strainer (BD Falcon, Franklin Lakes, NJ, USA). After skinning, the fibers were washed three times instead of only once and the measurement in the Oxygraph-2k was performed under normal air oxygen pressure without the usage of catalase and H_2O_2. 2 mg of muscle fibers were used for respiratory analysis. 2 mg liver were weighed and cut in small pieces before being placed in the Oxygraph-2k, digitonin was added to permeabilise the tissue. Measurements were performed as described above for mouse mitochondria. Cytochrome c effect was 4.4±1.9% for liver and 2.1±1.5% for muscle fibers.

2.2.11 Statistical analysis

Proteomics, lipidomics and high-resolution respirometry were performed with isolated mitochondria from 8 mice (n=8; due to logistical reasons respirometry was only measured with n=5 for isolated liver mitochondria). Follow-up respirometry for further characterization of the substrate preference was performed with another set of 5 mice (n=5 for liver and muscle mitochondria). For functional and western blot analyses, statistical significance was evaluated by a Student´s t-test using GraphPad Prism (GraphPad Software, La Jolla, CA, USA). A p-value <0.05 was considered significant. The open-source MultiExperiment Viewer software(44) was employed for heatmap generation using mean centered data pre-scaled to unit variance (UV). Multivariate Principal Component Analysis (PCA) was performed on the lipid concentrations per µg mitochondrial protein with SIMCA-P 11.5 (Umetrics, Umeå, Sweden). Data were UV scaled and log transformed using the auto transformation option. The content of individual PGs and CLs was divided by the sum of all PGs and CLs, respectively, to calculate the percental contribution of individual species. The sum of acyl chains within CLs was obtained by multiplying the content of individual CLs with the number of acyl chains within this CL (e.g., 1*(18:1)

and 3*(18:2) for CL(18:1)$(18:2)_3$) and also expressed as percentage. For the statistical analysis of lipidomics and proteomics data the Response Screening platform in JMP 13.0 (SAS, Cary, NC, USA) was used, considering an FDR p-value <0.05 as significant.

3. RESULTS

3.1 Mitochondria show tissue-specific protein compositions

First, we analysed liver and skeletal muscle mitochondrial protein composition by data-independent proteomics to elucidate the molecular basis for tissue-specific differences. Mitochondria were isolated from mouse liver and upper hind limb muscles consisting mainly of type 2 fibers. Proteins with known mitochondrial localization according to the Mitominer 4.0 database (48) accounted for 89% and 86% of total detected signal intensity in liver and muscle mitochondria, respectively. The analysis revealed a quite distinct tissue-specific mitochondrial protein pattern (Figure 1). In accordance with organ function, muscle mitochondria contained a higher percentage of proteins related to oxidative phosphorylation, ATP synthesis, and pyruvate decarboxylation (Figure 1 a, b). Two ATP synthase subunits (ATPA, ATPB) and ADP/ATP translocase 1 (ADT1) accounted for 17% of total protein intensity in muscle mitochondria (Figure 1 d). Enzymes of the citric acid cycle were also more abundant in muscle mitochondria. The percentage of proteins related to β-oxidation, in contrast, was higher in liver than in muscle (Figure 1 a, b). Mitochondrial 3-ketoacyl-CoA thiolase (THIM), which catalyzes the last step of β-oxidation, was the second most abundant protein in liver mitochondria (Figure 1 c). Proteins involved in ketogenesis, gluconeogenesis, and amino acid metabolism were also higher in liver mitochondria (Figure 1 a, b).

The mitochondrial abundance of several subunits of the respiratory chain was different between the tissues (Figure 2). Almost all subunits of complex I and several of III and V, but also some subunits of complex IV were more abundant in skeletal muscle than in liver mitochondria (Figure 2). For complex II, succinate dehydrogenase B (SDHB) and succinate dehydrogenase C (C560) were higher in

muscle mitochondria, whereas SDHA was higher in liver. The electron transfer flavoproteins ETFA, ETFB, and ETFD which mediate the reduction of ubiquinone by $FADH_2$ derived from β-oxidation and amino acid degradation were also more abundant in liver than in muscle mitochondria.

We also had a closer look on the abundance of mitochondrial proteins determining the route of pyruvate or acetyl-CoA towards mitochondrial oxidation or biosynthetic pathways (Figure 3). Proteomics analyses revealed higher abundance of the proteins of the pyruvate dehydrogenase complex (PDC) in muscle. Citrate synthase (CISY) was also higher in muscle than in liver mitochondria. In contrast, pyruvate carboxylase (PYC) was highly abundant in liver mitochondria, which links pyruvate to gluconeogenesis. Mitochondrial tricarboxylate transport protein (TXTP), which exports citrate for cytosolic acetyl-CoA production, was high abundant in liver mitochondria. This is well in line with the high rate of fatty acid synthesis and ketogenesis in the liver. As shown in Figure 1, most enzymes of the TCA cycle were more abundant in muscle mitochondria, while several enzymes involved in β-oxidation were more abundant in liver mitochondria. Of note, in addition to SDHA, succinate-CoA ligase (SUCB2) showed higher abundance in liver mitochondria (Figure 3).

Comparison of the results obtained by proteomics with western blot analysis revealed a reasonable overlap indicating a good suitability of the widely used antibodies to capture differences in mitochondrial protein abundance. The data showed higher abundance of citrate synthase and of four out of five electron transport chain complexes in muscle compared with liver mitochondria (Figure 4). The difference in complex III did not reach statistical significance (Figure 4 e). We also investigated the abundance of some of these proteins in total tissue lysates by western blot analyses (Figure 5 a). Similar to isolated mitochondria, citrate synthase (CISY) and pyruvate dehydrogenase (ODP) were higher in skeletal muscle, while pyruvate carboxylase (PYC) was pronouncedly higher in the liver (Figure 5 b-d). Western blot analysis of ACADM and ECHA confirmed the higher abundance of enzymes of β-oxidation in liver tissue compared to skeletal muscle tissue (Figure 5 e, f).

3.2 Mitochondria from skeletal muscle show higher phospholipid levels than from liver

Next, the lipid profile of the isolated mouse liver and skeletal muscle mitochondria was investigated by UHPLC-MS/MS analyses. The tissue origin had no major effect on the total number of detected lipid species (Supplementary Figure A.1), but tissue differences in the lipid profiles were obvious, as shown by multivariate principal component analysis (Supplementary Figure A.2). In the direction of the first principal component a pronounced separation of the clustered hepatic and skeletal muscle-derived mitochondrial samples could be seen. Muscle mitochondria had a higher total lipid content than liver mitochondria (316±49 pmol lipids/µg total mitochondrial protein versus 221±39 pmol/µg). Accordingly, most lipid classes were more abundant in muscle mitochondria (Table 1; Figure 6).

To assess differences in membrane lipid composition of liver and muscle mitochondria, data were normalized to total phospho- and sphingolipid content, which was 261±41 pmol/µg mitochondrial protein in muscle mitochondria and 172±35 pmol/µg mitochondrial protein in liver mitochondria (Table 1). In skeletal muscle the total and the relative amounts of the mitochondria signature lipid cardiolipin (CL) and of the CL precursor phosphatidylglycerol (PG) were significantly higher than in liver, as were phosphatidylethanolamines (PE) and phosphatidylserines (PS) (Table 1). PEs together with phosphatidylcholines (PC) were the major phospholipids in mitochondrial membranes, accounting for 84±0.8% of total phospholipids in liver and 77±0.8% in muscle mitochondria (Table 1). Ceramide, phosphatidylinositol and PC were significantly higher in liver than in muscle mitochondria (Table 1). The contribution of sphingomyelin to membrane lipid content of mitochondria derived from liver or muscle was equal (Table 1).

3.3 Cardiolipins have a different acyl chain composition in muscle and liver mitochondria

CL are the only mitochondria-specific lipids. To compare the patterns of CL and of their precursor lipids PG, levels of individual species were normalized to the sum of CL (Figure 7). The most abundant CL species in muscle contained four 18:2 acyl chains (25.5% ± 4.3% in muscle vs. 13.6% ± 3.2% in liver

mitochondria). In both tissues, 18:2 was the most abundant acyl chain present in CL (55.2% of all acyl chains in muscle vs. 47.3% in liver mitochondria, Table 2). A striking finding was the higher amount of 22:6 acyl chains in CL of skeletal muscle mitochondria compared to liver. 22:6 was found in four of the 24 CL species and accounted for 4.6% of all CL acyl chains in muscle and 1.7% in liver (Table 2). Interestingly, PGs containing 22:6 acyl chains were significantly lower or below detection limit in muscle, possibly indicating a preferential channeling of these acyl chains into CL (Figure 7). CL containing 20:4 acyl chains were more abundant in liver compared to muscle mitochondria.

Differences in protein composition between liver and skeletal muscle are linked to tissue-specificity of mitochondrial function and respiratory substrate preferences

To elucidate the impact of these differing protein and lipid fingerprints on respiration, we analysed mouse liver and skeletal muscle mitochondria by high-resolution respirometry. Striking differences were observed analyzing the complex I and complex II-linked substrates pyruvate and succinate (Figure 8 a, b). Muscle mitochondria respired significantly more after the addition of pyruvate, while no increase in respiration of liver mitochondria was detectable. This is in consistency with the higher abundance of the proteins of the pyruvate dehydrogenase complex (PDC) in muscle revealed by proteomic analyses, which links the glycolytic pathway to the TCA cycle and by that provides NADH for complex I. In contrast, liver mitochondria respired significantly more after adding the complex II-associated substrate succinate. Accordingly, the contribution of complex II-associated substrate oxidation to maximal respiration on complex I and II substrates was higher in liver as evident after addition of the complex I inhibitor rotenone. Using glutamate as complex I-linked substrate instead of pyruvate revealed the same differences between liver and muscle mitochondria (Figure 8 c-e). To avoid any effects of the combination with the β-oxidation substrate octanoylcarnitine, pyruvate-driven respiration was also studied before adding octanoylcarnitine (Figure 8 f, g). Again, muscle mitochondria proved to be more prone to the provided complex I-linked substrate pyruvate than liver and comparable results were obtained with glutamate (Figure 8 h). The subsequent addition of

396 octanoylcarnitine led only in liver mitochondria to a further increase in respiration, independent of
397 the complex I substrate used (Figure 8 i).

398 It has to be taken into account, that the mouse skeletal muscle mitochondria were isolated from the
399 upper hind limbs representing mostly fast type 2 fibers (4). However, the observed differences in
400 complex I and II-linked substrate respiration were confirmed in human skeletal muscle fibers isolated
401 from vastus lateralis muscle which represent a mix of slow type 1 and fast type 2 fibers
402 (Figure 8 j-l) (46). Human muscle fibers showed higher respiration on complex I substrate pyruvate,
403 while human liver homogenate showed higher respiration on complex II substrate succinate. These
404 data underline that the different contribution of complex I and II to maximal respiration in liver and
405 muscle mitochondria is of relevance in mice and humans and not restricted to fast muscle fibers.

406

407 **4. DISCUSSION**

408 Here we report a multi-omics approach to provide an overall mitochondrial molecular fingerprint on
409 the levels of lipids and proteins for muscle and liver tissue and additionally link it to respiratory
410 function. Our work indicates a tissue-specific mitochondrial respiratory profile with distinctly
411 different respiratory complex I and II substrate preferences of mitochondria from liver compared to
412 skeletal muscle. Muscle mitochondria showed high respiration on complex I-linked substrates
413 pyruvate and glutamate, whereas liver mitochondria respired less on these substrates but showed
414 high respiration on complex II-linked substrate succinate. Our detailed investigation of the tissue-
415 specific respiration on the substrates pyruvate, glutamate, succinate and octanoylcarnitine extend
416 previous reports obtained with isolated mitochondria of a type 2 diabetes rat model (Goto-Kakizaki
417 rats) and whole muscle and liver tissue from mice (16, 20). Moreover, the integration of proteomics
418 and lipidomics analyses underlines these divergent metabolic activities of muscle and liver
419 mitochondria and highlights the molecular determinants.

The enzymes responsible for the different metabolic routes of pyruvate in mitochondria showed a tissue-specific distribution. Complex I-linked substrate pyruvate can be shuttled into different metabolic routes in mitochondria. After conversion to acetyl-CoA by pyruvate dehydrogenase complex, it is further oxidized in the TCA cycle, thereby feeding electrons into the respiratory chain. Acetyl-CoA is also shuttled into anabolic pathways (e.g. ketogenesis, fatty acid synthesis). Pyruvate can also be metabolized to oxaloacetate by pyruvate carboxylase, which is then used for gluconeogenesis. Proteins of the pyruvate dehydrogenase complex were found to be higher in muscle lysates and muscle mitochondria. Citrate synthase which catalyzes the entry of acetyl-CoA into the TCA cycle by condensating it with oxaloacetate to citrate, was highly abundant in muscle tissue and mitochondria compared to liver. In contrast, we detected almost no pyruvate carboxylase in muscle tissue and mitochondria, whereas it was prominently detected in liver, the main site for gluconeogenesis. Additionally, ketogenic enzymes were highly abundant in liver mitochondria but not in muscle. These results clearly indicate that in muscle pyruvate is mainly used for complex I-dependent ATP production, while in liver mitochondria it serves as substrate for gluconeogenesis and ketogenesis. The other used complex I-linked substrate glutamate enters the TCA cycle as α-ketoglutarate, a step catalyzed by glutamate dehydrogenase (DHE3), thereby producing NADH. Notably, even though DHE3 was the fifth most abundant protein in liver mitochondria, only a low increase in O_2 flux after glutamate addition was detected in liver mitochondria. This indicates that feeding electrons via complex I into the electron transport chain has a low capacity in liver mitochondria, whereas in skeletal muscle it is the preferred entry. In contrast, electrons delivered via complex II from oxidation of succinate or via electron transfer flavoproteins from β-oxidation to ubiquinone strongly activate respiration of liver mitochondria.

The tissue-specificity of the mitochondrial respiratory complexes detected in our study and in part described in previous reports (10, 37) further substantiated the differences in respiration. Muscle mitochondria are characterized by a higher contribution of almost all subunits of complex I to the total proteome compared to liver, and a higher contribution of most subunits of complex III, IV and

ATP synthase. The higher phosphorylating respiration in liver mitochondria after the addition of the complex II-linked substrate succinate is apparently not based on differences in the abundance of complex II subunits, since only SDHA showed higher abundance in liver mitochondria, while SDHB and SDHC were higher in muscle. However, the two most abundant SDH assembly factors SDHF 1 and 2 were higher in liver mitochondria (Supplement B). These are necessary for maturation and maintaining SDH activity (52). SDH activity is also necessary to shuttle the amino acids valine, isoleucine, methionine and threonine towards gluconeogenesis. They are degraded to propionyl-CoA, which is converted to succinyl-CoA. The enzyme responsible for this last step, methymalonyl-CoA mutase, was 7 times more abundant in liver than in muscle mitochondria (Supplement B). The proteome data also underline the preference of the liver to use fatty acids and branched-chain amino acids as substrates for oxidation and feeding electrons via $FADH_2$ into the electron transport chain. This includes the higher abundance of enzymes involved in β-oxidation and branched chain amino acid oxidation and the higher abundance of electron transfer flavoproteins ETFA, ETFB and ETFD. Together, our data demonstrate the dominant function of muscle mitochondria to generate ATP, which is in particular needed during physical activity due to the high ATP consumption of the contracting muscle. Muscle tissue has not only a higher density of mitochondria (3) but the muscle mitochondria are also tailored to achieve a high capacity of oxidative phosphorylation. The preferred usage of complex I-linked substrates is of advantage as a more efficient way of electron transfer for ATP production, since all three proton-pumping complexes are involved. The high capacity of liver mitochondria for oxidation of succinate mirrors that SDH is not only required for feeding electrons into the electron transport chain, but to maintain gluconeogenesis.

Our data on mitochondrial phospholipid content and composition underline the tissue-specific different functions of muscle and liver mitochondria. We found that levels of the mitochondrial signature lipid CL, as well as its precursor PG, were significantly higher in skeletal muscle. CLs are mainly located in the inner membrane of mitochondria (17) facilitating tight membrane folding and cristae formation (3, 40). CLs directly interact with respiratory chain complexes (26, 55) and the ATP

synthase (1), thereby regulating ATP production. Genetic disorders with impact on CL metabolism result in depleted CL levels and mitochondrial dysfunction such as Barth´s syndrome and underscore the essential role of CL (30). Furthermore, CL is a critical component for stabilizing respiratory supercomplexes from complexes I, III, and IV, which in turn are thought to increase the efficiency of electron transfer (25, 35). Thus, the higher content of CL found in muscle mitochondria is probably responsible for the higher density of cristae described for muscle mitochondria (3) and the higher capacity for supercomplex assembly including complex I (45, 55) both of which support ATP generation. Notably, exercise training has been shown to increase muscle CL content and supercomplex formation (12, 31), underlining the importance of CL for the high oxidative phosphorylation capacity of the muscle.

CL are glycerol-bridged, dimeric phospholipids substituted with four fatty acyl side chains, which opens up a huge number of possible molecular lipid species, that has just started to be unraveled (28). The underlying process of CL remodelling is of extraordinary selectivity, exemplified by the detected differences in CL species in muscle and liver. While 18:2 is the dominating acyl chain in both tissues, the relative amount of $(18:2)_4$-CL is higher in muscle than in liver mitochondria, and this CL species has been associated with higher activity of respiratory complexes supporting our hypothesis of muscle mitochondria being more specified for oxidative phosphorylation than liver (9, 49). In skeletal muscle mitochondria, the second most abundant polyunsaturated fatty acid (PUFA) in CL was 22:6. CL containing 22:6 acyl chains might be essential to provide the high oxidative phosphorylation flexibility in muscle mitochondria. This hypothesis is supported by an improved ADP sensitivity found in human skeletal muscle mitochondria with an increased 22:6 acyl chain content after dietary supplementation (15). Exercise training was also shown to increase 22:6 acyl chains in muscle phospholipids in mice and in humans (2, 47). In mouse heart, even more than 50% of all CL species contained 22:6 acyl chains (32). PE levels were also significantly higher in muscle than in liver mitochondria. This lipid class might also play a role in mitochondrial function, since a depletion of mitochondrial PE in cells led to defective ETC complexes and a decreased respiratory capacity (51).

Even though far from being completely understood, the tissue-specific lipid and acyl chain content of liver and muscle mitochondrial lipids presumably supports the adaptation to the different metabolic tasks of both tissues.

Our comparison of liver and muscle mitochondria is mainly based on using a mixture of upper hind limb muscles from mice. These muscles mainly represent fast type 2 fibers, whereas slow type 1 fibers are rare in mice and restricted to a few muscles such as the soleus (46). Thus, we cannot exclude that comparing liver mitochondria with slow muscle fiber-derived mitochondria would lead to different results. However, we confirmed our results on substrate preference and different contribution of complex I and II to maximal respiration in liver tissue homogenates and muscle fibers from humans. Human vastus lateralis muscle contain both slow and fast fibers with similar distribution and using this mixed fiber type led to similar results. This indicates that the tissue-specific differences in mitochondrial respiration are also present when comparing liver and mixed muscle fibers. Moreover, the tissue-specific differences were found not only in isolated mitochondria but when the cellular localization and organization of mitochondria is preserved and when human instead of mouse samples are investigated. Together, we provide clear evidence that our data are of relevance for human mitochondria from muscle and liver tissue. As a next step, it would be of great interest to compare subsarcolemmal and intermyofibrillar mitochondria of skeletal muscle using this comprehensive investigation of proteomics, lipidomics and respiration data.

The tissue-specific differences in mitochondrial equipment and function could play a role in disease pathologies and form an essential basis for specified drug targeting. Metformin is one of the most common therapeutics for treating type 2 diabetes. A still widely proposed action of metformin is the inhibition of complex I in liver mitochondria however at millimolar concentrations (8, 36). Considering our findings that complex I-linked respiration in liver is of minor relevance, an inhibition thereof as explanation for the efficacy of metformin seems unlikely. Notably, very recent research highlighted alternative mechanisms of the action of metformin on hepatic gluconeogenesis as inhibition of glycerol-3-phosphate dehydrogenase (27) and inhibition of fructose-1,6-

524 bisphosphatase (18). The attempts to identify the target of metformin illustrates how an advanced
525 knowledge about mitochondria and their distinct tissue-specificities can support drug development.

526 Following this line, liver and skeletal muscle mitochondria appear to have different capacities to
527 compensate for the metabolic disturbances in obesity and diabetes. In skeletal muscle some
528 evidence points to a decreased mitochondrial function in diabetes (22, 33, 41). This is in contrast to
529 an increased mitochondrial function in liver of insulin resistant, diabetic or non-alcoholic fatty liver
530 disease (NAFLD) patients (23, 50). Future research will show whether some of the observed tissue-
531 specific differences play a role in this different adaptation of muscle and liver mitochondria to insulin
532 resistance and diabetes.

533 **5. CONCLUSIONS**

534 We present a comprehensive investigation of isolated mitochondria from skeletal muscle and liver
535 covering not only molecular but also functional analyses, to obtain tissue-specific protein and lipid
536 profiles and the consequences for respiration. In muscle mitochondria, we found a high contribution
537 of respiratory complex I, III, IV and ATP synthase subunits to the mitochondrial proteome and a high
538 content of CL, in particular of $(18:2)_4$-CL and 22:6 containing CL, in accordance with the high
539 specialization of these mitochondria to rapidly and drastically increase the rate of ATP production
540 whenever necessary. On the other hand, liver mitochondria are adapted to generate metabolites for
541 biosynthetic pathways of gluconeogenesis and ketogenesis while relying on fatty acids and amino
542 acids for oxidative phosphorylation. The results can build the base for a deeper understanding of
543 mitochondrial function and dysfunction in states of health or disease by providing a global coverage
544 of mitochondria. The investigation of tissue-specificities of mitochondria might also help to interpret
545 the often controversial findings in mitochondrial research. Thus, our data show how mitochondria
546 are specialized in a tissue-specific fashion in order to ensure efficient utilization of available
547 substrates.

548

6. ACKNOWLEDGEMENTS

The authors are grateful for the excellent technical support provided by Heike Runge from the University Hospital Tübingen, Tübingen, Germany.

Funding sources:

JL was supported by a research fellow grant of the Alexander von Humboldt Foundation. We gratefully acknowledge the financial support from the German Federal Ministry of Education and Research (BMBF) to the German Centre for Diabetes Research (DZD e.V.; No. 01GI0925), from the National Key Research and Development Program of China (2017YFC0906900), and the National Natural Science Foundation of China (No. 21874130) and (No. 21435006) to GX and the support by the Ministerium für Kultur und Wissenschaft des Landes Nordrhein-Westfalen, the Regierende Bürgermeister von Berlin - inkl. Wissenschaft und Forschung, and the BMBF to LK and AS.

MH LK CW RL designed the study, MH performed mouse studies, CH, LJ, GX designed and performed lipidomics analyses, CvT and SH designed and performed proteomics analyses, LK, CH, DB, AB, HZ, AK, AP performed or contributed to respirometry analyses, LK performed Western blot analyses, LK MH SH LK AS CW RL analysed and reviewed data, HUH MH CW RL supervised research and edited the manuscript, LK CW RL wrote the manuscript.

7. DISCLOSURE

The authors declare no competing interests.

573

574

575 **8. REFERENCES**

576 1. **Acehan D, Malhotra A, Xu Y, Ren M, Stokes DL, and Schlame M.** Cardiolipin affects the
577 supramolecular organization of ATP synthase in mitochondria. *Biophys J* 100: 2184-2192, 2011.

578 2. **Andersson A, Sjodin A, Hedman A, Olsson R, and Vessby B.** Fatty acid profile of skeletal
579 muscle phospholipids in trained and untrained young men. *Am J Physiol Endocrinol Metab* 279: E744-
580 751, 2000.

581 3. **Benard G, Faustin B, Passerieux E, Galinier A, Rocher C, Bellance N, Delage J-P, Casteilla L,**
582 **Letellier T, and Rossignol R.** Physiological diversity of mitochondrial oxidative phosphorylation. *Am J*
583 *Physiol Cell Physiol* 291: C1172-C1182, 2006.

584 4. **Bloemberg D and Quadrilatero J.** Rapid determination of myosin heavy chain expression in
585 rat, mouse, and human skeletal muscle using multicolor immunofluorescence analysis. *PLoS One* 7:
586 e35273-e35273, 2012.

587 5. **Chen S, Hoene M, Li J, Li Y, Zhao X, Häring H-U, Schleicher ED, Weigert C, Xu G, and**
588 **Lehmann R.** Simultaneous extraction of metabolome and lipidome with methyl tert-butyl ether from
589 a single small tissue sample for ultra-high performance liquid chromatography/mass spectrometry. *J*
590 *Chromatogr A* 1298: 9-16, 2013.

591 6. **Claypool SM.** Cardiolipin, a critical determinant of mitochondrial carrier protein assembly
592 and function. *Biochim Biophys Acta* 1788: 2059-2068, 2009.

593 7. **DeFronzo RA, Jacot E, Jequier E, Maeder E, Wahren J, and Felber JP.** The effect of insulin on
594 the disposal of intravenous glucose. Results from indirect calorimetry and hepatic and femoral
595 venous catheterization. *Diabetes* 30: 1000-1007, 1981.

596 8. **El-Mir MY, Nogueira V, Fontaine E, Averet N, Rigoulet M, and Leverve X.** Dimethylbiguanide
597 inhibits cell respiration via an indirect effect targeted on the respiratory chain complex I. *J Biol Chem*
598 275: 223-228, 2000.

599 9. **Fajardo VA, McMeekin L, Saint C, and LeBlanc PJ.** Cardiolipin linoleic acid content and
600 mitochondrial cytochrome c oxidase activity are associated in rat skeletal muscle. *Chem Phys Lipids*
601 187: 50-55, 2015.

602 10. **Forner F, Foster LJ, Campanaro S, Valle G, and Mann M.** Quantitative proteomic comparison
603 of rat mitochondria from muscle, heart, and liver. *Mol Cell Proteomics* 5: 608-619, 2006.

604 11. **Furler SM, Cooney GJ, Hegarty BD, Lim-Fraser MY, Kraegen EW, and Oakes ND.** Local factors
605 modulate tissue-specific NEFA utilization: assessment in rats using 3H-(R)-2-bromopalmitate.
606 *Diabetes* 49: 1427-1433, 2000.

607 12. **Greggio C, Jha P, Kulkarni SS, Lagarrigue S, Broskey NT, Boutant M, Wang X, Conde Alonso**
608 **S, Ofori E, Auwerx J, Cantó C, and Amati F.** Enhanced Respiratory Chain Supercomplex Formation in
609 Response to Exercise in Human Skeletal Muscle. *Cell Metab* 25: 301-311, 2017.

610 13. **Grosche A, Hauser A, Lepper MF, Mayo R, von Toerne C, Merl-Pham J, and Hauck SM.** The
611 proteome of native adult Müller glial cells from murine retina. *Mol Cell Proteomics* 15: 462-480,
612 2016.

613 14. **Heden TD, Neufer PD, and Funai K.** Looking Beyond Structure: Membrane Phospholipids of
614 Skeletal Muscle Mitochondria. *Trends Endocrinol Metab* 27: 553-562, 2016.

615 15. **Herbst EA, Paglialunga S, Gerling C, Whitfield J, Mukai K, Chabowski A, Heigenhauser GJ,**
616 **Spriet LL, and Holloway GP.** Omega-3 supplementation alters mitochondrial membrane composition
617 and respiration kinetics in human skeletal muscle. *J Physiol* 592: 1341-1352, 2014.

618 16. **Holmstrom MH, Iglesias-Gutierrez E, Zierath JR, and Garcia-Roves PM.** Tissue-specific
619 control of mitochondrial respiration in obesity-related insulin resistance and diabetes. *Am J Physiol*
620 *Endocrinol Metab* 302: E731-739, 2012.

17. **Horvath SE and Daum G.** Lipids of mitochondria. *Prog Lipid Res* 52: 590-614, 2013.

18. **Hunter RW, Hughey CC, Lantier L, Sundelin EI, Peggie M, Zeqiraj E, Sicheri F, Jessen N, Wasserman DH, and Sakamoto K.** Metformin reduces liver glucose production by inhibition of fructose-1-6-bisphosphatase. *Nat Med* 24: 1395, 2018.

19. **Johnson DT, Harris RA, French S, Blair PV, You J, Bemis KG, Wang M, and Balaban RS.** Tissue heterogeneity of the mammalian mitochondrial proteome. *Am J Physiol Cell Physiol* 292: C689-697, 2007.

20. **Jorgensen W, Jelnes P, Rud KA, Hansen LL, Grunnet N, and Quistorff B.** Progression of type 2 diabetes in GK rats affects muscle and liver mitochondria differently: pronounced reduction of complex II flux is observed in liver only. *Am J Physiol Endocrinol Metab* 303: E515-523, 2012.

21. **Kappler L, Li J, Häring H-U, Weigert C, Lehmann R, Xu G, and Hoene M.** Purity matters: A workflow for the valid high-resolution lipid profiling of mitochondria from cell culture samples. *Sci Rep* 6: 21107, 2016.

22. **Kelley DE, He J, Menshikova EV, and Ritov VB.** Dysfunction of Mitochondria in Human Skeletal Muscle in Type 2 Diabetes. *Diabetes* 51: 2944-2950, 2002.

23. **Koliaki C, Szendroedi J, Kaul K, Jelenik T, Nowotny P, Jankowiak F, Herder C, Carstensen M, Krausch M, Knoefel WT, Schlensak M, and Roden M.** Adaptation of hepatic mitochondrial function in humans with non-alcoholic Fatty liver is lost in steatohepatitis. *Cell Metab* 21: 739-746, 2015.

24. **Lanza IR and Sreekumaran Nair K.** Regulation of skeletal muscle mitochondrial function: genes to proteins. *Acta Physiologica* 199: 529-547, 2010.

25. **Lapuente-Brun E, Moreno-Loshuertos R, Acin-Perez R, Latorre-Pellicer A, Colas C, Balsa E, Perales-Clemente E, Quiros PM, Calvo E, Rodriguez-Hernandez MA, Navas P, Cruz R, Carracedo A, Lopez-Otin C, Perez-Martos A, Fernandez-Silva P, Fernandez-Vizarra E, and Enriquez JA.** Supercomplex assembly determines electron flux in the mitochondrial electron transport chain. *Science* 340: 1567-1570, 2013.

646 26. **Lee Y, Willers C, Kunji ERS, and Crichton PG.** Uncoupling protein 1 binds one nucleotide per
647 monomer and is stabilized by tightly bound cardiolipin. *Proc Natl Acad Sci USA* 112: 6973-6978, 2015.

648 27. **Madiraju AK, Erion DM, Rahimi Y, Zhang X-M, Braddock DT, Albright RA, Prigaro BJ, Wood**
649 **JL, Bhanot S, MacDonald MJ, Jurczak MJ, Camporez J-P, Lee H-Y, Cline GW, Samuel VT, Kibbey RG,**
650 **and Shulman GI.** Metformin suppresses gluconeogenesis by inhibiting mitochondrial
651 glycerophosphate dehydrogenase. *Nature* 510: 542, 2014.

652 28. **Maguire JJ, Tyurina YY, Mohammadyani D, Kapralov AA, Anthonymuthu TS, Qu F,**
653 **Amoscato AA, Sparvero LJ, Tyurin VA, Planas-Iglesias J, He R-R, Klein-Seetharaman J, Bayır H, and**
654 **Kagan VE.** Known unknowns of cardiolipin signaling: The best is yet to come. *Biochim Biophys Acta,*
655 *Mol Cell Biol Lipids* 1862: 8-24, 2017.

656 29. **McGarry JD and Foster DW.** Regulation of hepatic fatty acid oxidation and ketone body
657 production. *Annu Rev Biochem* 49: 395-420, 1980.

658 30. **McKenzie M, Lazarou M, Thorburn DR, and Ryan MT.** Mitochondrial respiratory chain
659 supercomplexes are destabilized in Barth Syndrome patients. *J Mol Biol* 361: 462-469, 2006.

660 31. **Menshikova EV, Ritov VB, Dube JJ, Amati F, Stefanovic-Racic M, Toledo FGS, Coen PM, and**
661 **Goodpaster BH.** Calorie Restriction-induced Weight Loss and Exercise Have Differential Effects on
662 Skeletal Muscle Mitochondria Despite Similar Effects on Insulin Sensitivity. *J Gerontol A Biol Sci Med*
663 *Sci* 73: 81-87, 2018.

664 32. **Minkler PE and Hoppel CL.** Separation and characterization of cardiolipin molecular species
665 by reverse-phase ion pair high-performance liquid chromatography-mass spectrometry. *J Lipid Res*
666 51: 856-865, 2010.

667 33. **Mogensen M, Sahlin K, Fernstrom M, Glintborg D, Vind BF, Beck-Nielsen H, and Hojlund K.**
668 Mitochondrial respiration is decreased in skeletal muscle of patients with type 2 diabetes. *Diabetes*
669 56: 1592-1599, 2007.

34. **Mootha VK, Bunkenborg J, Olsen JV, Hjerrild M, Wisniewski JR, Stahl E, Bolouri MS, Ray HN, Sihag S, Kamal M, Patterson N, Lander ES, and Mann M.** Integrated analysis of protein composition, tissue diversity, and gene regulation in mouse mitochondria. *Cell* 115: 629-640, 2003.

35. **Osman C, Voelker DR, and Langer T.** Making heads or tails of phospholipids in mitochondria. *J Cell Biol* 192: 7-16, 2011.

36. **Owen MR, Doran E, and Halestrap AP.** Evidence that metformin exerts its anti-diabetic effects through inhibition of complex 1 of the mitochondrial respiratory chain. *Biochem J* 348 Pt 3: 607-614, 2000.

37. **Pagliarini DJ, Calvo SE, Chang B, Sheth SA, Vafai SB, Ong S-E, Walford GA, Sugiana C, Boneh A, Chen WK, Hill DE, Vidal M, Evans JG, Thorburn DR, Carr SA, and Mootha VK.** A Mitochondrial Protein Compendium Elucidates Complex I Disease Biology. *Cell* 134: 112-123, 2008.

38. **Pearce J.** Fatty acid synthesis in liver and adipose tissue. *Proc Nutr Soc* 42: 263-271, 1983.

39. **Pesta D and Gnaiger E.** High-resolution respirometry: OXPHOS protocols for human cells and permeabilized fibers from small biopsies of human muscle. *Methods Mol Biol* 810: 25-58, 2012.

40. **Phan MD and Shin K.** Effects of cardiolipin on membrane morphology: a Langmuir monolayer study. *Biophys J* 108: 1977-1986, 2015.

41. **Phielix E, Schrauwen-Hinderling VB, Mensink M, Lenaers E, Meex R, Hoeks J, Kooi ME, Moonen-Kornips E, Sels J-P, Hesselink MKC, and Schrauwen P.** Lower intrinsic ADP-stimulated mitochondrial respiration underlies in vivo mitochondrial dysfunction in muscle of male type 2 diabetic patients. *Diabetes* 57: 2943-2949, 2008.

42. **Postic C, Dentin R, and Girard J.** Role of the liver in the control of carbohydrate and lipid homeostasis. *Diabetes Metab* 30: 398-408, 2004.

43. **Rothman DL, Magnusson I, Katz LD, Shulman RG, and Shulman GI.** Quantitation of hepatic glycogenolysis and gluconeogenesis in fasting humans with 13C NMR. *Science* 254: 573-576, 1991.

44. **Saeed AI, Sharov V, White J, Li J, Liang W, Bhagabati N, Braisted J, Klapa M, Currier T, Thiagarajan M, Sturn A, Snuffin M, Rezantsev A, Popov D, Ryltsov A, Kostukovich E, Borisovsky I, Liu Z, Vinsavich A, Trush V, and Quackenbush J.** TM4: A free, open-source system for microarray data management and analysis. *Biotechniques* 34: 374-378, 2003.

45. **Schägger H and Pfeiffer K.** Supercomplexes in the respiratory chains of yeast and mammalian mitochondria. *EMBO J* 19: 1777-1783, 2000.

46. **Schiaffino S.** Fibre types in skeletal muscle: a personal account. *Acta Physiologica* 199: 451-463, 2010.

47. **Senoo N, Miyoshi N, Goto-Inoue N, Minami K, Yoshimura R, Morita A, Sawada N, Matsuda J, Ogawa Y, Setou M, Kamei Y, and Miura S.** PGC-1alpha-mediated changes in phospholipid profiles of exercise-trained skeletal muscle. *J Lipid Res* 56: 2286-2296, 2015.

48. **Smith AC and Robinson AJ.** MitoMiner v3.1, an update on the mitochondrial proteomics database. *Nucleic Acids Res* 44: D1258-1261, 2016.

49. **Sullivan EM, Pennington ER, Sparagna GC, Torres MJ, Neufer PD, Harris M, Washington J, Anderson EJ, Zeczycki TN, and Brown DA.** Docosahexaenoic acid lowers cardiac mitochondrial enzyme activity by replacing linoleic acid in the phospholipidome. *J Biol Chem* 293: 466-483, 2018.

50. **Takamura T, Misu H, Matsuzawa-Nagata N, Sakurai M, Ota T, Shimizu A, Kurita S, Takeshita Y, Ando H, Honda M, and Kaneko S.** Obesity upregulates genes involved in oxidative phosphorylation in livers of diabetic patients. *Obesity (Silver Spring, Md)* 16: 2601-2609, 2008.

51. **Tasseva G, Bai HD, Davidescu M, Haromy A, Michelakis E, and Vance JE.** Phosphatidylethanolamine deficiency in mammalian mitochondria impairs oxidative phosphorylation and alters mitochondrial morphology. *J Biol Chem* 288: 4158-4173, 2013.

52. **Van Vranken JG, Na U, Winge DR, and Rutter J.** Protein-mediated assembly of succinate dehydrogenase and its cofactors. *Crit Rev Biochem Mol Biol* 50: 168-180, 2015.

718 53. **Wallace DC.** Bioenergetic origins of complexity and disease. *Cold Spring Harb Symp Quant*
719 *Biol* 76: 1-16, 2011.

720 54. **Wiśniewski JR, Zougman A, Nagaraj N, and Mann M.** Universal sample preparation method
721 for proteome analysis. *Nature Methods* 6: 359, 2009.

722 55. **Zhang M, Mileykovskaya E, and Dowhan W.** Gluing the respiratory chain together.
723 Cardiolipin is required for supercomplex formation in the inner mitochondrial membrane. *J Biol Chem*
724 277: 43553-43556, 2002.

725
726

9. TABLES

Table 1: Absolute lipid class levels in isolated mitochondria from liver and muscle and as percentage of the total membrane lipid (ML) amount with n= 7 for liver and 8 for muscle mitochondria. Data are presented as means ± standard deviation (SD). CER= ceramides, CL= cardiolipins, FFA= free fatty acids, LPC= lysophosphatidylcholines, LPE= lysophosphatidylethanolamines, LPI= lysophosphatidylinositols, PC= phosphatidylcholines, PC-P= phosphatidylcholine plasmalogens, PE= phosphatidylethanolamines, PE-P= phosphatidylethanolamine plasmalogens, PG= phosphatidylglycerols, PI= phosphatidylinositols, PL= total phospholipids, PS= phosphatidylserines, PS-P= phosphatidylserine plasmalogens, SM= sphingomyelins, TG= triacylglycerols. The Response Screening platform in JMP 13.0 (SAS, Cary, NC, USA) was used, considering an FDR p-value <0.05 as significant.

lipid class	mean liver [pmol/µg]	SD liver	mean muscle [pmol/µg]	SD muscle	FDR p value M vs. L	mean liver / ML[%]	SD liver	mean muscle / ML[%]	SD muscle	FDR p value
CER	0.786	0.051	0.854	0.074	0.090	0.48	0.14	0.33	0.06	0.023
CL	12.028	3.068	31.208	6.324	<0.001	6.93	0.74	11.90	0.96	<0.001
FFA	35.089	14.890	42.932	9.528	0.274					
LPC	0.948	0.166	3.108	0.668	<0.001					
LPE	0.659	0.131	4.666	0.907	<0.001					
LPI	0.083	0.026	0.076	0.027	0.631					
PC	98.772	18.064	125.505	18.441	0.025	57.71	1.70	48.64	0.80	<0.001
PC-P	0.012	0.005	1.282	0.296	<0.001					
PE	44.466	10.334	66.485	10.503	0.003	25.82	1.08	27.90	0.66	0.001
PE-P	0.119	0.042	6.386	1.442	<0.001					
PG	1.066	0.339	4.918	1.250	<0.001	0.61	0.08	1.86	0.18	<0.001
PI	10.430	3.117	11.110	1.949	0.631	5.97	0.76	4.25	0.28	0.001
PS	2.549	0.332	4.974	0.441	<0.001	1.60	0.21	2.01	0.11	0.001
PS-P	0.156	0.075	0.224	0.097	0.191					
SM	0.626	0.220	1.072	0.495	0.076	0.36	0.07	0.41	0.17	0.496
TG	13.825	3.555	11.277	1.334	0.109					

Table 2: Acyl chain composition of cardiolipins from mitochondria derived from mouse liver and muscle, FA= fatty acyl chain. The Response Screening platform in JMP 13.0 (SAS, Cary, NC, USA) was used, considering an FDR p-value <0.05 as significant.

FA	liver [%]	SD liver	muscle [%]	SD muscle	FDR p value
12:0	3.88	0.89	2.76	0.59	0.011
15:0	3.88	0.89	2.76	0.59	0.011
16:0	1.09	0.07	0.61	0.14	0.003
16:1	8.15	0.69	6.68	0.81	0.010
18:0	5.24	1.01	4.95	0.67	0.643
18:1	10.73	0.57	8.19	0.57	0.003
18:2	47.27	4.65	55.24	4.23	0.011
20:0	0.04	0.03	1.69	0.22	0.003
20:1	0.54	0.13	0.46	0.15	0.227
20:2	0.57	0.13	0.17	0.05	0.003
20:3	2.87	0.31	1.91	0.14	0.003
20:4	5.45	1.05	1.25	0.15	0.003
20:5	4.62	0.42	4.47	0.12	0.209
21:0	0.18	0.11	0.19	0.02	0.515
22:1	1.09	0.26	0.92	0.30	0.227
22:2	2.48	0.50	1.25	0.22	0.003
22:5	0.04	0.03	1.69	0.22	0.003
22:6	1.74	0.47	4.64	0.69	0.003
23:2	0.12	0.04	0.18	0.04	0.015

10. LEGENDS TO FIGURES

Figure 1: **Composition of mitochondrial proteome from mouse liver and skeletal muscle.** Upper panel: relative contribution of different mitochondrial processes to the total protein intensity in a: liver and b: skeletal muscle mitochondria. Lower panel: contribution of the five most abundant proteins to the total detected protein intensity in c: liver and d: skeletal muscle mitochondria (n= 8). Colors in c and d correspond to a and b. ACON= aconitate hydratase; ADT1= ADP/ATP translocase 1; ALDH2= aldehyde dehydrogenase; ATPA= ATP synthase subunit alpha; ATPB= ATP synthase subunit beta; DHE3= glutamate dehydrogenase 1; MDHM= mitochondrial malate dehydrogenase; THIM= mitochondrial 3-ketoacyl-CoA thiolase.

Figure 2: **Proteins of the respiratory chain complexes with different relative abundance in the mitochondrial proteome of mouse liver and skeletal muscle.** CI-CIV= complex I to IV; CV= ATP synthase; Cyt c= cytochrome c; ETF= electron transfer flavoprotein; Q= coenzyme Q_{10} (ubiquinone). Solely significantly different proteins are shown. Colors represent higher abundance of proteins in muscle (blue) and liver mitochondria (red) (n= 8). The Response Screening platform in JMP 13.0 (SAS, Cary, NC, USA) was used, considering an FDR p-value <0.05 as significant. For details, see Supplement B.

Figure 3: **Proteins of pyruvate and fatty acid oxidation with different relative abundance in the mitochondrial proteome of mouse liver and skeletal muscle.** Solely significantly different proteins are shown. Colors represent higher abundance of proteins in muscle (blue) and liver mitochondria (red) (n= 8). The Response Screening platform in JMP 13.0 (SAS, Cary, NC, USA) was used, considering an FDR p-value <0.05 as significant. For details, see Supplement B.

Figure 4: **Analysis of electron transport chain complexes in purified mitochondria of mouse liver and skeletal muscle**. a: representative western blot of 4 mitochondria isolations per tissue. Equal protein amounts (30 µg) of total cell lysates and mitochondria were loaded on the same blot to determine the protein levels before mitochondrial enrichment. b: mitochondrial citrate synthase (CISY) was assessed as common mitochondrial marker protein. c-g: for the detection of the electron transport chain complexes, an antibody cocktail was used against NDUB8 (complex I), SDHB (complex II), QCR2 (complex III), and ATPA (complex V). A separate antibody was used for complex IV (COX4; F). Signals were normalized to total protein abundance determined via stain-free 2,2,2-trichloroethanol. Histograms show the densitometric quantifications of western blots (n=8, mean of "muscle" set to 1). Data are presented as means ± standard deviation (SD). tmP= total mitochondrial protein, rel= relative. Statistical significance was evaluated by Student´s t-test.

Figure 5: **Quantity of individual proteins related to energy metabolism in tissue lysates of mouse liver and skeletal muscle** analysed by western blot (a) and densitometric quantification (b-f). A representative western blot with 4 out of 8 tissue lysates is shown. Mitochondrial citrate synthase (CISY) was used as a mitochondrial marker (b). ODP= pyruvate dehydrogenase, PYC= pyruvate carboxylase, ACADM= medium-chain acyl-CoA dehydrogenase, ECHA=hydroxyacyl-CoA dehydrogenase/3-ketoacyl-CoA thiolase/enoyl-CoA hydratase (trifunctional protein), alpha subunit. ODP (c) and PYC (d) were assessed to investigate pyruvate metabolism. ACADM and ECHA were used to assess β-oxidation (e+f). Histograms show the sums of the densitometric quantifications of western blots (Mean of "muscle" was set to 1, n=8). Signals are normalized to total protein abundance. Data are presented as means ± standard deviation (SD). tP= total protein, rel= relative. Statistical significance was evaluated by a Student´s t-test.

Figure 6: **Heatmap visualization of the total amounts of the different lipid (sub-)classes in mitochondrial samples** from mouse liver (n= 7) and skeletal muscle (n= 8, lipid content per µg protein). Each column represents one animal. Values were centered to the mean of the respective lipid class and scaled to unit variance. White color shows values close to the mean of the lipid class and red- and blue-colored values are higher and lower, respectively, than the mean. CER= ceramide,

CL= cardiolipin, FFA= free fatty acid, LPC= lysophosphatidylcholine, LPE= lysophosphatidylethanolamine, LPI= lysophosphatidylinositol, PC= phosphatidylcholine, PC-P= phosphatidylcholine plasmalogen, PE= phosphatidylethanolamine, PE-P= phosphatidylethanolamine plasmalogen, PG= phosphatidylglycerol, PI= phosphatidylinositol, PS= phosphatidylserine, PS-P= phosphatidylserine plasmalogen, SM= sphingomyelin, TG= triacylglycerol. The Response Screening platform in JMP 13.0 (SAS, Cary, NC, USA) was used, considering an FDR p-value <0.05 as significant.

Figure 7: **Acyl chain patterns of mitochondrial cardiolipin (CL) and its precursor phosphatidylglycerol (PG) from mouse skeletal muscle and liver** (n= 8, lipid content as percentage of the total CL (left) or PG (right) amount). Data are presented as means ± standard deviation (SD). The Response Screening platform in JMP 13.0 (SAS, Cary, NC, USA) was used, considering an FDR p-value <0.05 as significant. p-values: *<0.05, **<0.01, ***<0.001.

Figure 8: **Respiratory analyses of mouse liver and skeletal muscle mitochondria (a-i) and human liver tissue homogenate and skeletal muscle fibers (j-l) on an Oxygraph-2k**: a-e: respiration of mouse liver and skeletal muscle mitochondria with consecutive addition of malate (M), octanoylcarnitine (Oct), ADP (D), pyruvate (P) or glutamate (G), and succinate (S). U= uncoupled respiration using the protonophore carbonylcyanide p-trifluoromethoxyphenylhydrazone; Rot= rotenone (complex I inhibitor); a+b: titration protocol, exemplarily shown for measurements with P; c: increase of phosphorylating respiration with P or G (complex I substrates); d: increase of phosphorylating respiration with succinate (complex II substrate); e: ratio of maximal uncoupled complex II respiration to total maximal uncoupled respiration with complex I and II substrates; n=5 for liver mitochondria and n=8 for muscle mitochondria isolated from 8 mice. f-i: respiration of mouse liver and skeletal muscle mitochondria with consecutive addition of M, P or G, D, and Oct as substrates. f+g: titration protocol, exemplarily shown for P; h: increase of respiration after ADP injection; i: increase of phosphorylating respiration with Oct. n=5 for liver and muscle mitochondria isolated from 5 mice not identical with a-e; j-l: Titration protocol performed as shown in a and b with human liver tissue homogenate (3 donors) and skeletal muscle fibers (8 donors); j: increase of phosphorylating respiration with P; k: increase of phosphorylating respiration with S; l: ratio of maximal uncoupled complex II respiration to total maximal uncoupled respiration with complex I and II substrates. Data are presented as means ± standard deviation (SD). Statistical significance was evaluated by Student´s t-test.

11. FIGURES

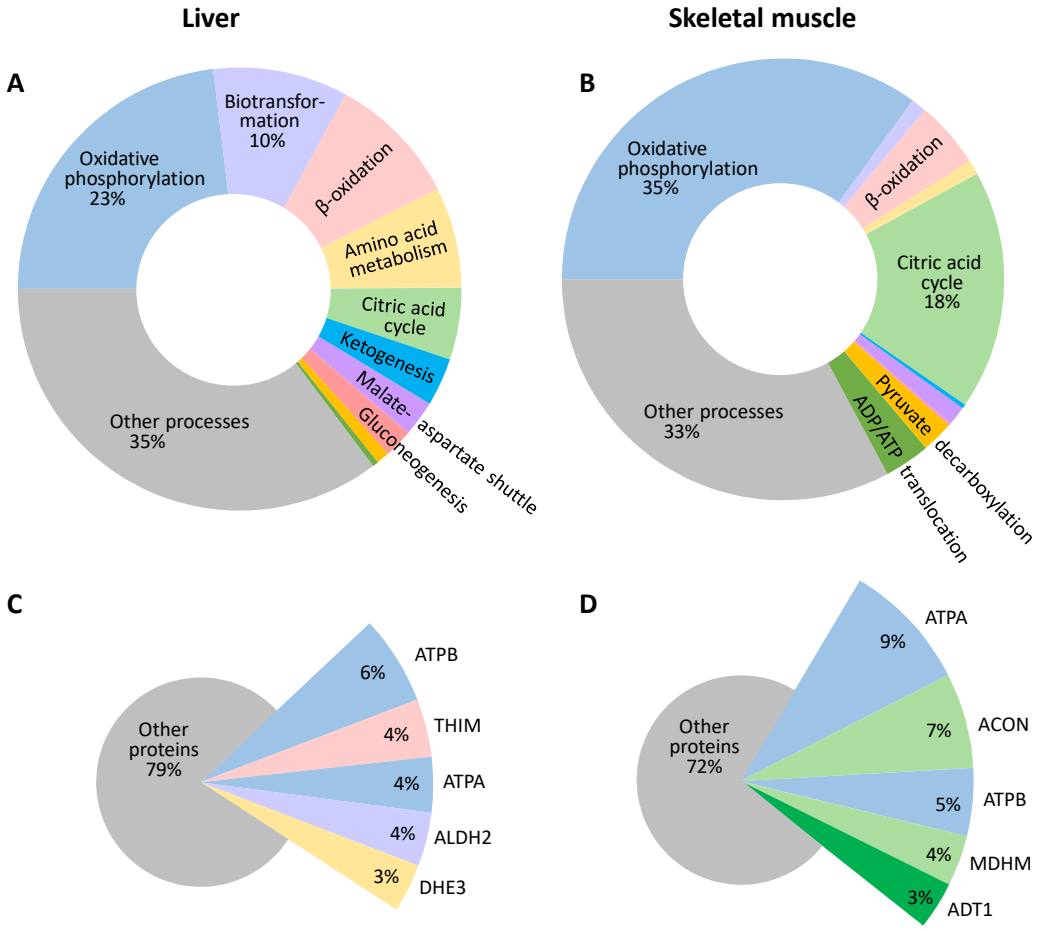

Figure 1

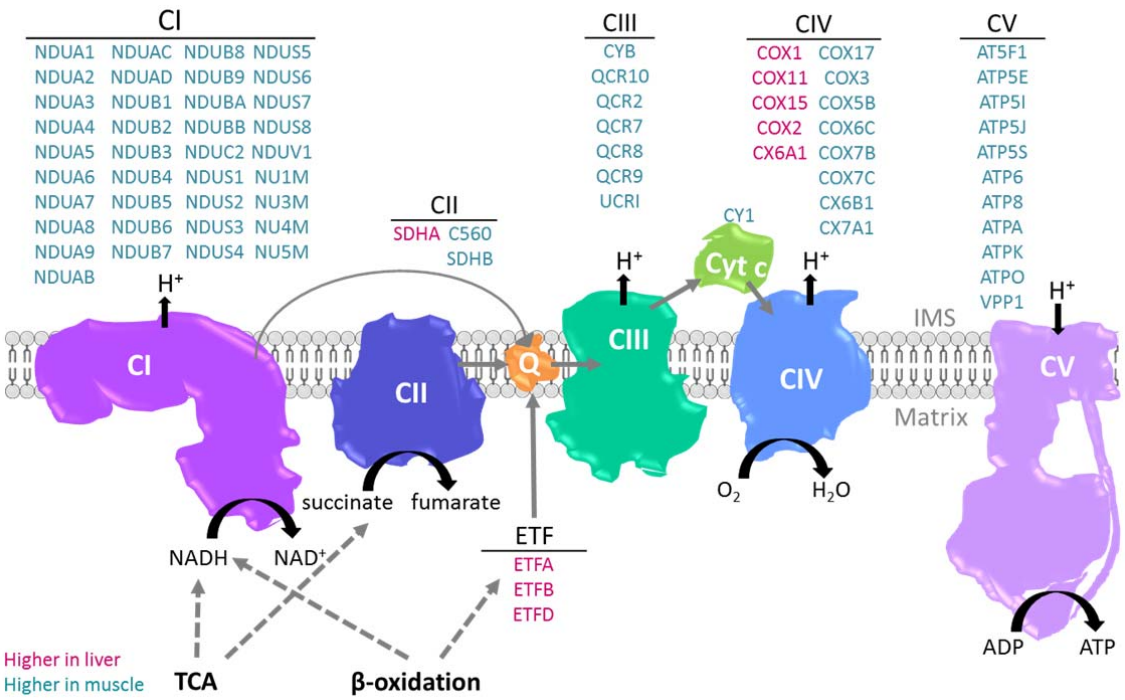
CI
NDUA1 NDUAC NDUB8 NDUS5
NDUA2 NDUAD NDUB9 NDUS6
NDUA3 NDUB1 NDUBA NDUS7
NDUA4 NDUB2 NDUBB NDUS8
NDUA5 NDUB3 NDUC2 NDUV1
NDUA6 NDUB4 NDUS1 NU1M
NDUA7 NDUB5 NDUS2 NU3M
NDUA8 NDUB6 NDUS3 NU4M
NDUA9 NDUB7 NDUS4 NU5M
NDUAB
CII
SDHA C560
SDHB
CIII
CYB
QCR10
QCR2
QCR7
QCR8
QCR9
UCRI
CIV
COX1 COX17
COX11 COX3
COX15 COX5B
COX2 COX6C
CX6A1 COX7B
COX7C
CX6B1
CX7A1
CV
AT5F1
ATP5E
ATP5I
ATP5J
ATP5S
ATP6
ATP8
ATPA
ATPK
ATPO
VPP1
CY1
Cyt c
H+
IMS
Matrix
Q
succinate
fumarate
NADH
NAD+
ETF
ETFA
ETFB
ETFD
O2
H2O
ADP
ATP
Higher in liver
Higher in muscle
TCA
β-oxidation

Figure 2

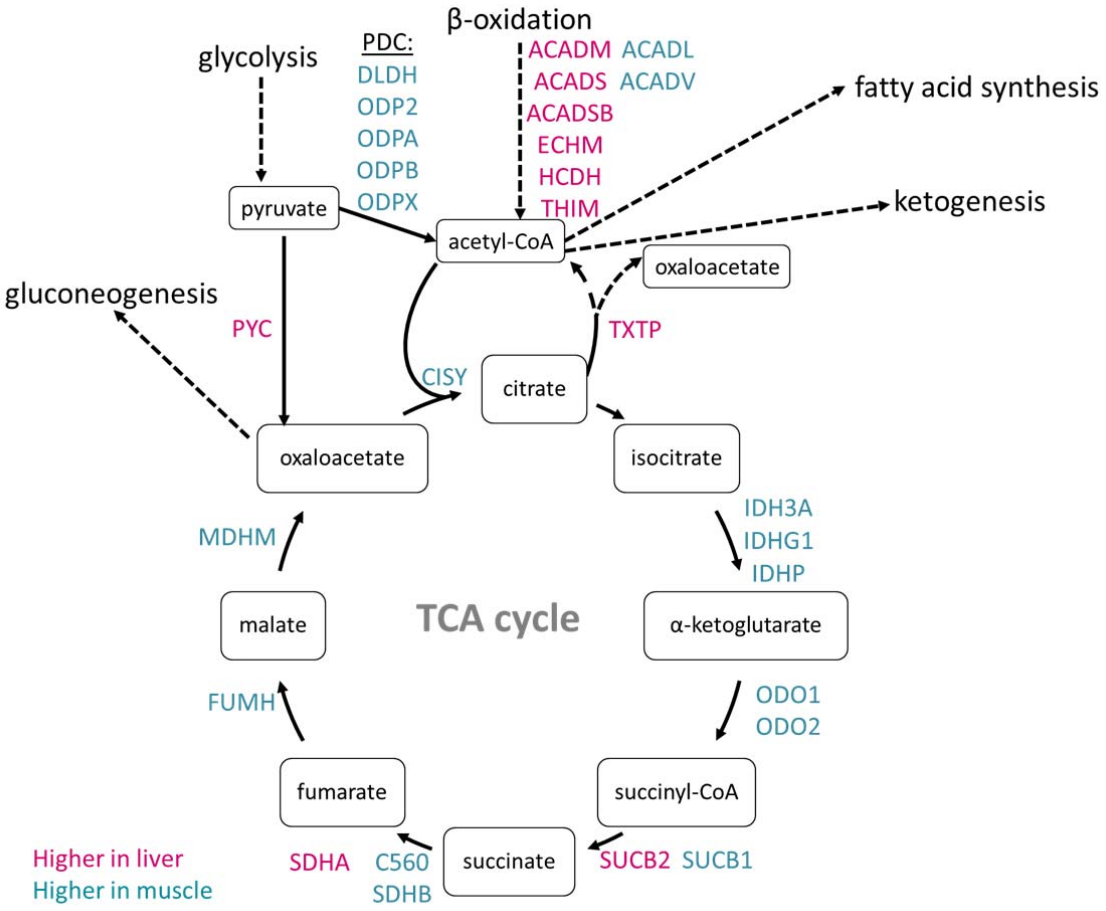
β-oxidation
glycolysis
PDC:
DLDH
ODP2
ODPA
ODPB
ODPX
ACADM ACADL
ACADS ACADV
ACADSB
ECHM
HCDH
THIM
fatty acid synthesis
ketogenesis
pyruvate
acetyl-CoA
oxaloacetate
gluconeogenesis
PYC
TXTP
CISY
citrate
oxaloacetate
isocitrate
IDH3A
IDHG1
IDHP
MDHM
malate
TCA cycle
α-ketoglutarate
FUMH
ODO1
ODO2
fumarate
succinyl-CoA
Higher in liver
Higher in muscle
SDHA
C560
SDHB
succinate
SUCB2 SUCB1

Figure 3

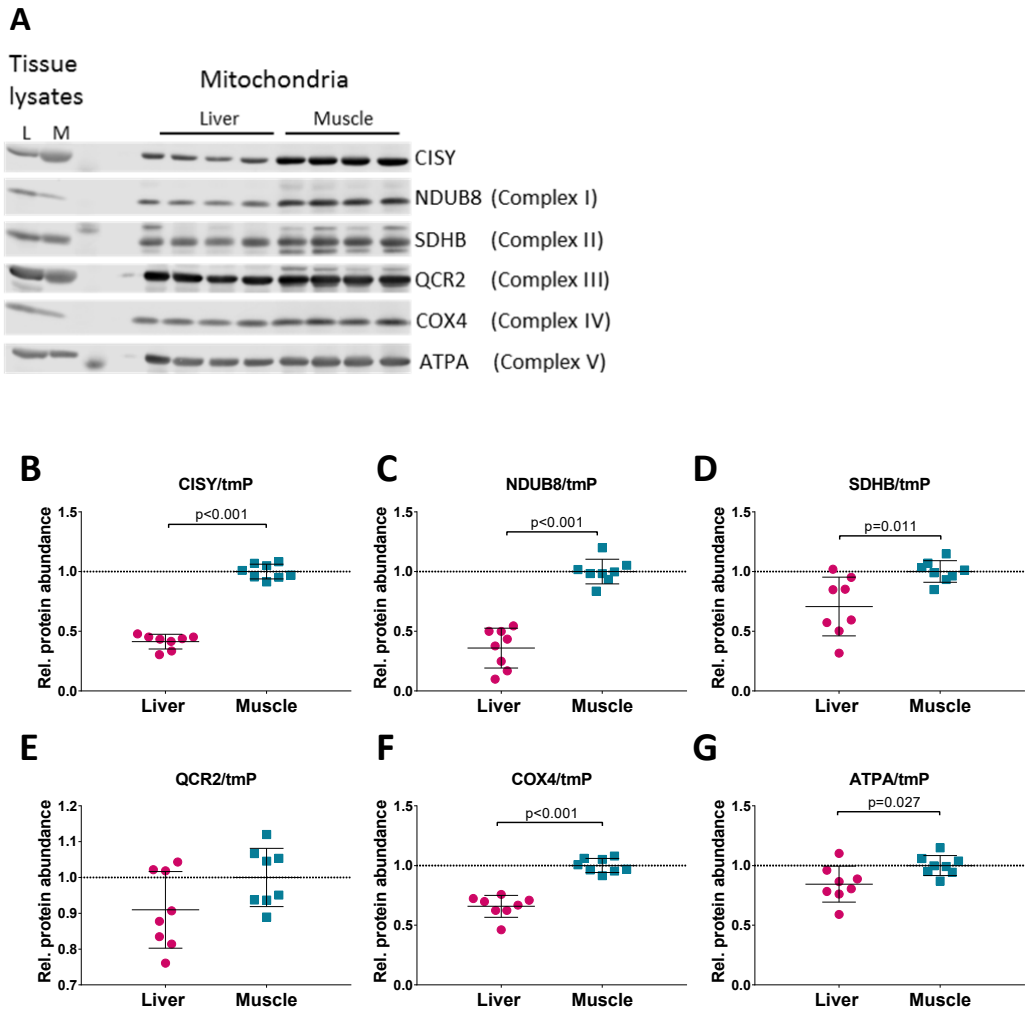
A
Tissue lysates
L M
Mitochondria
Liver
Muscle
CISY
NDUB8 (Complex I)
SDHB (Complex II)
QCR2 (Complex III)
COX4 (Complex IV)
ATPA (Complex V)
B
CISY/tmP
p<0.001
C
NDUB8/tmP
p<0.001
D
SDHB/tmP
p=0.011
E
QCR2/tmP
F
COX4/tmP
p<0.001
G
ATPA/tmP
p=0.027
Rel. protein abundance
Liver
Muscle

Figure 4

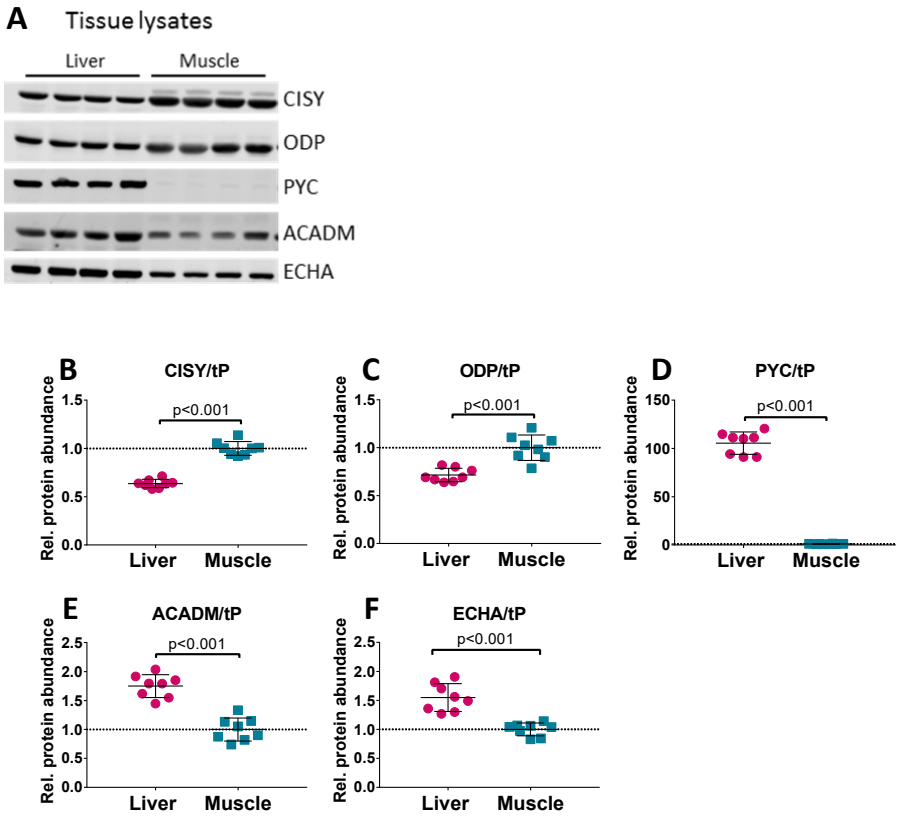

Figure 5

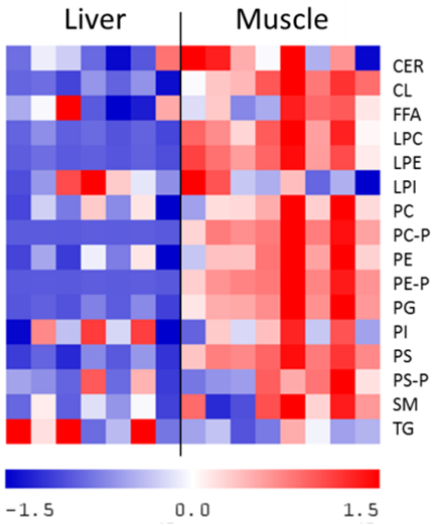

Figure 6

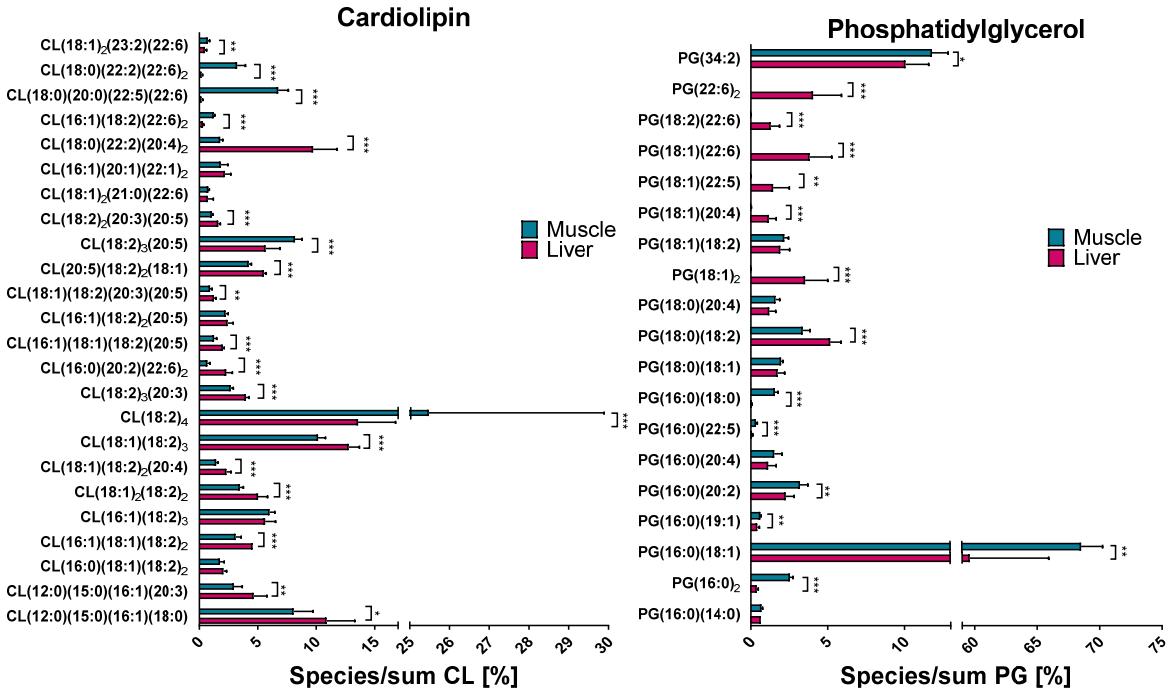

Figure 7

Figure 8: see next page

Mouse

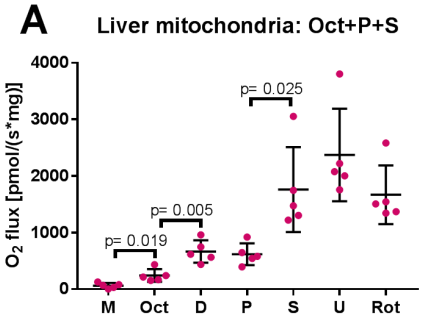
A
Liver mitochondria: Oct+P+S
O2 flux [pmol/(s*mg)]
4000
3000
2000
1000
0
p= 0.019
p= 0.005
p= 0.025
M
Oct
D
P
S
U
Rot

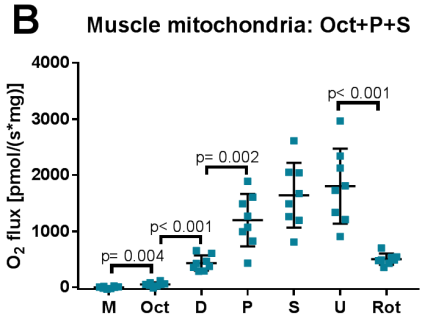
B
Muscle mitochondria: Oct+P+S
O2 flux [pmol/(s*mg)]
4000
3000
2000
1000
0
p= 0.004
p< 0.001
p= 0.002
p< 0.001
M
Oct
D
P
S
U
Rot

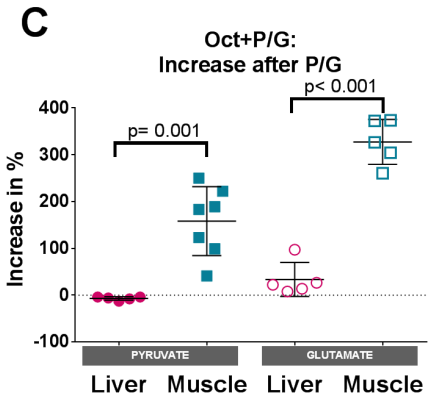
C
Oct+P/G:
Increase after P/G
Increase in %
400
300
200
100
0
-100
p= 0.001
p< 0.001
PYRUVATE
GLUTAMATE
Liver
Muscle
Liver
Muscle

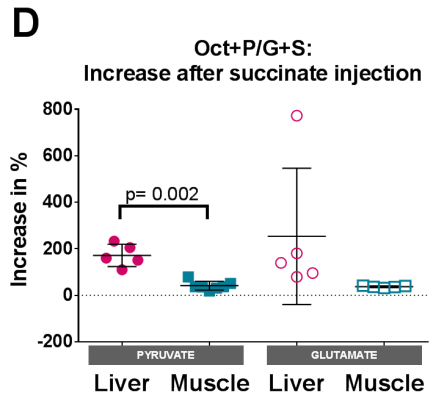
D
Oct+P/G+S:
Increase after succinate injection
Increase in %
800
600
400
200
0
-200
p= 0.002
PYRUVATE
GLUTAMATE
Liver
Muscle
Liver
Muscle

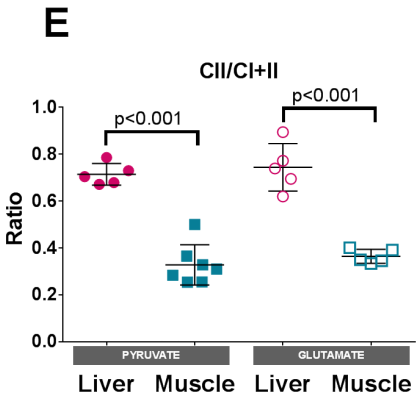
E
CII/CI+II
Ratio
1.0
0.8
0.6
0.4
0.2
0.0
p<0.001
p<0.001
PYRUVATE
GLUTAMATE
Liver
Muscle
Liver
Muscle

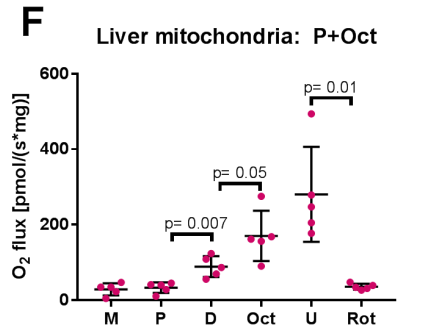
F
Liver mitochondria: P+Oct
O2 flux [pmol/(s*mg)]
600
400
200
0
p= 0.007
p= 0.05
p= 0.01
M
P
D
Oct
U
Rot

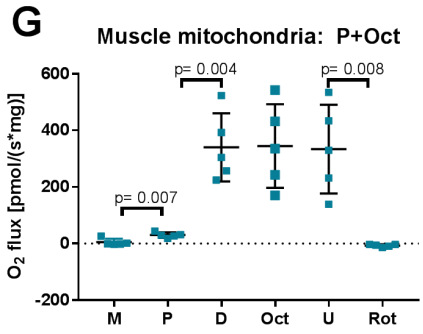
G
Muscle mitochondria: P+Oct
O2 flux [pmol/(s*mg)]
600
400
200
0
-200
p= 0.007
p= 0.004
p= 0.008
M
P
D
Oct
U
Rot

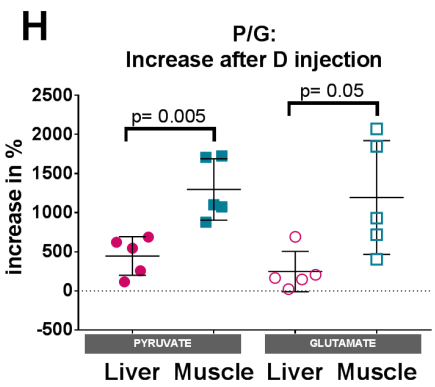
H
P/G:
Increase after D injection
increase in %
2500
2000
1500
1000
500
0
-500
p= 0.005
p= 0.05
PYRUVATE
GLUTAMATE
Liver
Muscle
Liver
Muscle

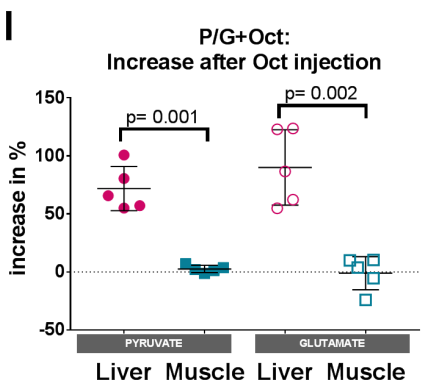
I
P/G+Oct:
Increase after Oct injection
increase in %
150
100
50
0
-50
p= 0.001
p= 0.002
PYRUVATE
GLUTAMATE
Liver
Muscle
Liver
Muscle

Human

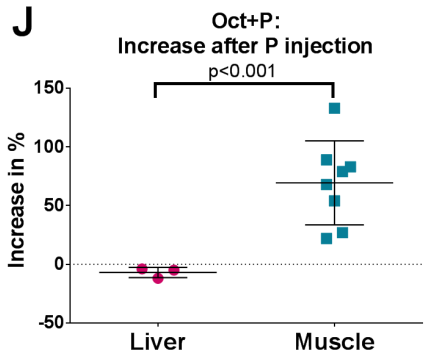
J
Oct+P:
Increase after P injection
Increase in %
150
100
50
0
-50
p<0.001
Liver
Muscle

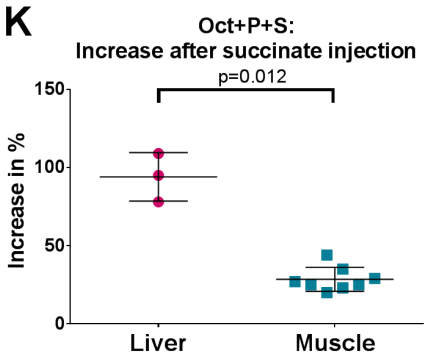
K
Oct+P+S:
Increase after succinate injection
Increase in %
150
100
50
0
p=0.012
Liver
Muscle

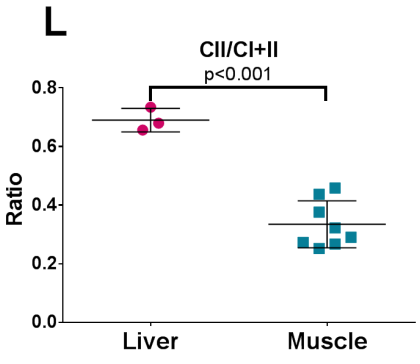
L
CII/CI+II
Ratio
0.8
0.6
0.4
0.2
0.0
p<0.001
Liver
Muscle

Supplement A

Linking bioenergetic function of mitochondria to tissue-specific molecular fingerprints

Lisa Kappler[1], Miriam Hoene[1], Chunxiu Hu[2], Christine von Toerne[3], Jia Li[1,4], Daniel Bleher[1], Christoph Hoffmann[1], Anja Böhm[5,6], Laxmikanth Kollipara[7], Hans Zischka[8,9], Alfred Königsrainer[10,11], Hans-Ulrich Häring[1,5,6], Andreas Peter[1,5,6], Guowang Xu[2], Albert Sickmann[7,12,13], Stefanie M Hauck[3,6], Cora Weigert[1,5,6], Rainer Lehmann[1,5,6*]

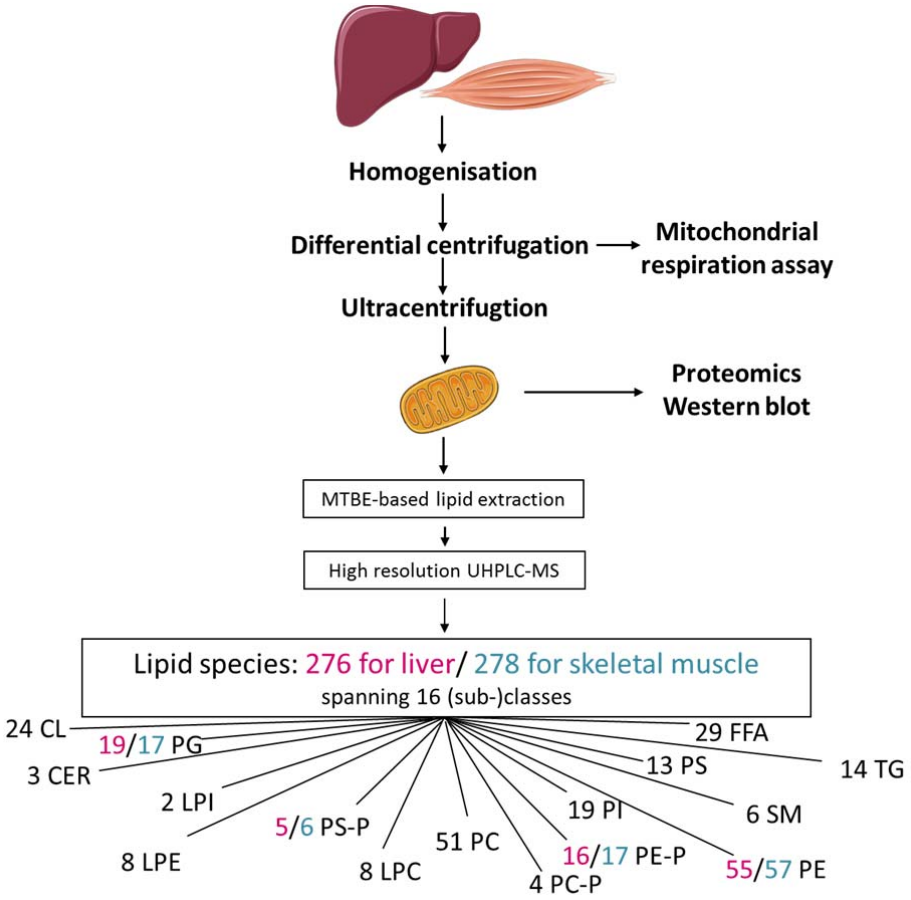

Supplementary Figure A.1: **Experimental workflow** from sample preparation to respiratory analyses, western blot and lipidomics analyses. See methods section for further details. CER= ceramide, CL= cardiolipin, FFA= free fatty acid, LPC= lysophosphatidylcholine, LPE= lysophosphatidylethanolamine, LPI= lysophosphatidylinositol, PC= phosphatidylcholine, PC-P = phosphatidylcholine plasmalogen, PE= phosphatidylethanolamine, PE-P= phosphatidylethanolamine plasmalogen, PG= phosphatidylglycerol, PI= phosphatidylinositol, PS= phosphatidylserine, PS-P= phosphatidylserine plasmalogen, SM= sphingomyelin, TG= triacylglycerol, MTBE= methyl tert-butyl ether, UHPLC-MS= ultra-high-performance liquid chromatography-mass spectrometry. Illustration uses elements from Servier Medical Art (www.servier.com).

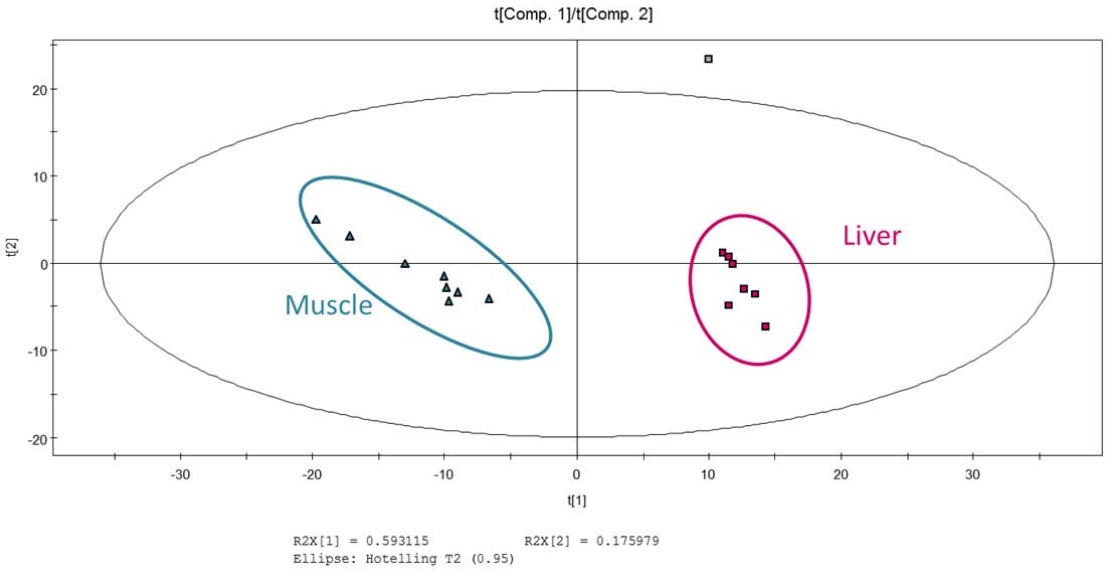

Supplementary Figure A.2: **Detection of distinct differences in the lipid fingerprint of skeletal muscle and liver.** Principal Component Analysis (PCA) scores plot of the first two principal components based on all detected lipids (relative standard deviation in the quality control samples <20% and after par scaling). The first component explains 59.3% of the variation and the second one 17.6%. Each spot represents one mitochondrial sample isolated from mouse liver or skeletal muscle using ultracentrifugation. One liver sample (grey labelled) was identified as outlier using Hotelling T 2 Ellipse (95% confidence limit) and excluded from further data analyses.